Scholars' Mine

2012

Process planning and control of functionally graded parts using freeze-form extrusion fabrication

Bradley Kenneth Deuser

Follow this and additional works at: https://scholarsmine.mst.edu/masters_theses

Part of the Mechanical Engineering Commons

Department:

Recommended Citation

PROCESS PLANNING AND CONTROL OF FUNCTIONALLY GRADED PARTS

USING FREEZE-FORM EXTRUSION FABRICATION

by

BRADLEY KENNETH DEUSER

A THESIS

Presented to the Faculty of the Graduate School of the

MISSOURI UNIVERSITY OF SCIENCE AND TECHNOLOGY

In Partial Fulfillment of the Requirements for the Degree

MASTER OF SCIENCE IN MECHANICAL ENGINEERING

2012

Approved by

Ming C. Leu, Advisor

Robert G. Landers

Greg E. Hilmas

PUBLICATION THESIS OPTION

This thesis consists of the following two articles that will or have been submitted for publication as follows:

Pages 3 – 20 have been published as pages 415-426 in the Proceedings of the *Twenty-Second International Solid Freeform Fabrication Symposium*, the University of Texas, Austin, TX, August 8-10 (2011).

Pages 21 – 50 are intended for submission to the *ASME Journal of Manufacturing Science and Engineering*.

ABSTRACT

Freeze-form Extrusion Fabrication (FEF) is an additive manufacturing technology that is capable of fabricating complex three-dimensional parts. FEF works by depositing an aqueous-based colloidal ceramic or metal paste in a layer-by-layer fashion below the freezing point of the aqueous medium as to rapidly freeze the paste. The FEF machine in the present study is equipped with three syringes and is capable of mixing each paste in a desired composition ratio by using an inline static mixer. Compensation for the transport delay caused by the static mixer is necessary; therefore, an algorithm was developed to apply a one-dimensional (1D) composition gradient to monolithic parts, adjusting the plunger velocities to account for the transport delay.

Control of extrusion-based additive manufacturing techniques is difficult due to the uncertainties of the paste properties such as entrapped air bubbles, inhomogeneity, and inconsistency of the paste rheology from batch to batch. Other challenges are present such as starting and stopping extrusion on demand (EOD) and steady-state velocity control of a coupled triple extruder system. These issues have been addressed with the development and implementation of a hybrid extrusion force-velocity controller.

ACKNOWLEDGMENTS

First I would like to express my gratitude to my advisor Dr. Ming Leu, co-advisor Dr. Robert Landers, and committee member Dr. Greg Hilmas for their support, technical expertise and valuable insight.

To Dr. Lie Tang and Dr. Jeremy Watts, I thank for their guidance and advice. Their skills and contributions have been invaluable for my success and the progress of the FEF project.

I would like to thank Robert J. Hribar, Joe Boze, Randall Lewis, Ken Gorman and George Green for their consultation and services to the FEF project. Their assistance with design problems and equipment upgrades allowed for multiple improvements to the FEF machine.

I would like to thank my graduate colleagues Mingyang Li, Ang Li, Aaron Thornton, Diego Garcia, and Hesam Zomorodi Moghadam for their help, support, and friendship throughout my graduate work.

My parents, Barbara and David Landolt Sr., have been a constant source of support with their words of encouragement and praise. I would not be where I am today without their guidance.

Last, but not least, I would like to thank my wife, Michelle, for her love, patience and understanding for the past several years throughout my undergraduate and graduate studies.

TABLE OF CONTENTS

LIST OF ILLUSTRATIONS

LIST OF TABLES

SECTION

Table   Page

INTRODUCTION

Additive manufacturing technology was first developed in the mid 1980's and quickly gained attention from its novel manufacturing approach. Initial methods such as Stereolithography [1], Fused Deposition Modeling [2], and 3D printing [3], allowed for rapid prototyping of complex three-dimensional polymer-based parts. Selective Laser Sintering [4,5] was originally developed for polymers, but was later utilized for fabrication of metal and ceramic-based parts. Materials such as ceramics and high temperature metals are difficult to process by traditional manufacturing techniques; therefore, additive manufacturing lends itself well to fabricating near-net-shape parts of complex geometry without costly and time-consuming mold preparation.

The next forefront in novel manufacturing techniques is the ability to incorporate multiple materials into a single part to take advantage of complimentary material properties, such as metal-reinforced ceramic composites. Materials must be graded between compositions to aid sintering, reduce the amount of residual stresses, and avoid potential delamination between materials [6]. In their current state, most of the popular metal and ceramic technologies are limited to single material (monolithic) part fabrication since they are sintering material from a single powder bed. Robocasting [7], Extrusion Freeform Fabrication [8], Shape Deposition Manufacturing [9], and Laser Metal Deposition [10] are better suited to build multiple-material parts since they are purely deposition-based processes.

This study considers a novel additive manufacturing technology called Freeze-form Extrusion Fabrication (FEF), which is capable of building three dimensional parts by depositing aqueous-based ceramic or metal-loaded pastes (45-50 vol. %) in a layer-by-layer manner in a sub-zero temperature environment. This minimizes the amount of binder necessary (2-4 vol. %), thus, making post-processing easier and more environmentally friendly [11-15]. This machine has been equipped with a triple-extruder mechanism to build complex geometry three-dimensional FGM parts.

The primary objective of this study is to develop a process planning and control scheme in order to build complex geometry parts with multiple materials. One of the more challenging aspects of extrusion-based freeform fabrication is the ability to start and

stop extrusion on demand [16]. Degassing of the ceramic or metal pastes via high-shear vacuum mixing minimizes the amount of air entrapped within the paste; however, some degree of compressibility is still present. An analytical process model was derived from first principles by Li et al. [17] that explains this behavior. In order to have good control of extrusion on demand an extrusion force controller is developed using this model to account for inconsistency in the amount of trapped air. By directly controlling the applied force to the plunger, the output extrusion rate is regulated. A plunger velocity controller is developed to regulate the output composition and a hybrid control scheme is developed to combine both controllers to intelligently control extrusion on demand for multiple-material parts. If excessive air is present in the paste due to improper loading of the syringe or preparation of the paste, large air bubbles may obstruct the nozzle and cause a disruption of extrusion flow rate. The hybrid extrusion force-velocity controller also corrects for this by using a scheme to switch between extrusion force and plunger velocity control to limit defects caused by air bubble release.

There is no readily available software to generate the path for functionally graded material parts. Skeinforge and other path planning software generate tool path data by first intersecting the STL file with multiple planes in the vertical direction to "slice" the part, and then the interior volume is filled with a random ordering of "loops" to minimize the number of start and stop commands. Several researchers such as Jackson et al. [18], Tan et al. [19,20], and Xu et al. [21] have proposed modeling techniques for FGM geometry parts. Automated tool path planning software for SFF fabrication of FGM parts does not exist due to the fact that each SFF process is unique in its fabrication medium as well as processing techniques; therefore, the method of fabricating multiple material parts is different for each machine. A one-dimensional gradient control algorithm is implemented in Paper I to demonstrate the capability of the FEF machine to fabricate FGM parts. In Paper II, the hybrid extrusion force-velocity controller capability is illustrated by fabricating an FGM part using tool path planning software and multiple compositions.

PAPER I

PROCESS PLANNING AND CONTROL FOR FUNCTIONALLY GRADED MATERIAL FABRICATION USING FREEZE-FORM EXTRUSION FABRICATION

Brad Deuser, Lie Tang, Jeff Geldmeier, Robert G. Landers, and Ming C. Leu

Department of Mechanical and Aerospace Engineering
Missouri University of Science and Technology, Rolla, MO 65409

1. ABSTRACT

Using multiple materials in additive manufacturing technologies is critical for building parts with functionally gradient geometries. In order to achieve a desired material gradient, an advanced process planning and control system is required. This paper details the development of a process planning method and control system for functionally graded material fabrication using a triple extruder Freeze-form Extrusion Fabrication (FEF) system including motion code generation, extruder dynamic modeling and control, and composition gradient control. The effect that extruding multiple materials from a single orifice via static mixing has on the time delay of the resulting mixture is taken into account for path planning, and this factor is incorporated into integrating motion codes with extrusion commands. The effectiveness of the proposed system is demonstrated by fabricating three-dimensional parts with desired gradient compositions using multiple materials.

2. INTRODUCTION

Additive manufacturing (AM) technology has advanced past the phase of rapid prototyping since its inception in the late 1980s and continues to evolve with the addition of novel building materials, advanced control schemes and the ability to fabricate intricate parts with complex internal cavities. These features, in combination with

increasing machine efficiency and little to no material waste, make AM technology desirable for building serviceable parts which are difficult and sometimes impossible to produce using traditional subtractive manufacturing processes. Among these advancements is the capability to build parts with multiple materials and functionally graded material (FGM) geometries.

Many attempts have been made by researchers to apply material composition gradients to solid CAD models using novel approaches such as heterogeneous object modeling [1], equal distance offset approach [2], and local composition control [3]. These methods decompose CAD models into their hierarchal elements in order to apply either material composition information to specific geometric features, or to apply graded material compositions through the cross section of a part. However, our project's initial efforts have focused on a simplified approach, which involves manipulating tool path motion codes generated by proprietary software (Stratasys Insight). This software is capable of generating tool path information for additive manufacturing applications with homogeneous materials, notably Fused Deposition Modeling (FDM) [4], but does not allow for multiple materials or functionally graded compositions. Therefore, in order to utilize this software, an algorithm was developed to integrate heterogeneous material composition gradient information with the pre-processed tool path from either Insight or a manually written G&M code to be used by extrusion-based additive manufacturing processes such as the Freeze-form Extrusion Fabrication process we are researching (Figure 1).
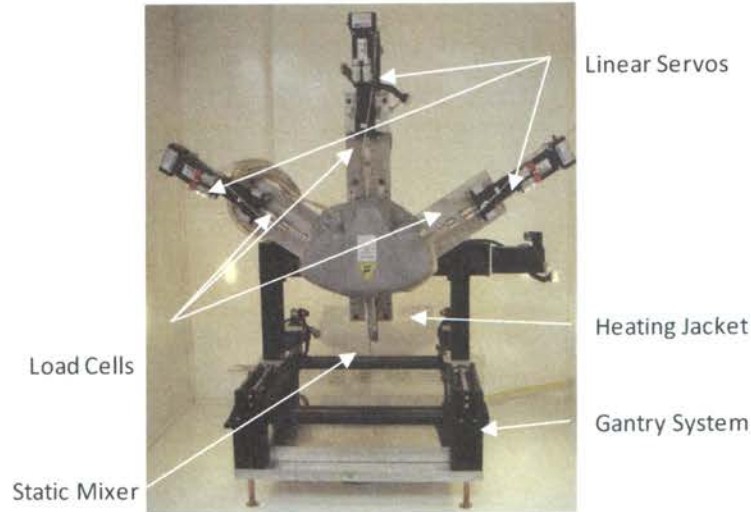
Figure 1: FEF machine with triple extruder mechanism.

Freeze-form Extrusion Fabrication (FEF) is a novel, layer-by-layer additive manufacturing process that builds three-dimensional (3D) parts by extruding aqueous-based colloidal pastes in an environment below the freezing point of water (-10° in our present study) in order to solidify the material as it exits the nozzle. This increases the build strength of each part and allows the FEF process to fabricate parts larger than that of room temperature extrusion processes (e.g., Robocasting [5] and Fab@Home [6]), and enables unsupported overhangs as much as 35° from the horizontal surface [7]. The triple-extruder FEF machine is capable of depositing three separate pastes from a single orifice by using an inline static mixer to blend together multiple materials (Figure 2). This passive mixing technique has been used to minimize the number of moving components

Figure 2: Static mixer (left) with mixing elements (right).

and controller complexity. However, it introduces a transport delay for changes in material composition that must be taken into account by the path planning software.

The research detailed in this paper outlines key issues for fabricating parts with multiple materials using the triple-extruder FEF system, which include: development of a general tracking velocity controller for the extrusion servo motors, taking into account the transport delay caused by the static mixer, and applying compositional gradients to

the fabrication of a 3D part. An analytical model of the transport delay was devised and then verified through experimental results, and graded parts were built using the developed process planning algorithm.

3. FEF EQUIPMENT

The triple extruder FEF machine is comprised of two coupled mechatronic systems: motion control and extrusion control (Figure 3). The three-axis motion gantry system is controlled using a Delta Tau Turbo PMAC card, which operates the FEF machine through G&M motion code. Extrusion is controlled with three Kollmorgen servo motors (AKM23D) using a National Instruments PXI chassis and LabVIEW. The two systems are coupled by sending analog signals from the Delta Tau system to the PXI-6025E LabVIEW multifunction

Figure 3: FEF control system schematic

board, which interprets the voltage into different commands (namely, the reference velocity of each plunger and the start and stop commands for extrusion on demand [5]). The PXI-6025E multifunction board also acquires signals from three load cells (Omega LC-305), which are attached to the end of each linear motion cylinder. These load cells track the amount of pressure being exerted on the plunger and serve as a regulation feedback device for extrusion on demand, monitoring paste quality and detecting clogging or the presence of air bubbles at the nozzle tip. The PXI system also houses a counter/timer board (PXI-6022) for velocity tracking using encoder measurements in quadrature mode for a maximum resolution of 0.2 μm/s. The final component on the PXI system is the analog output board (PXI-6711), which sends command voltages to the three linear cylinder amplifiers.

4. PROCESS MODELING AND CONTROL

4.1. Linear Cylinder Velocity Controller Design

Previous groups at Missouri S&T implemented extrusion force control to regulate the extrusion velocity [9-13] and achieved much success in doing so for a single-extruder FEF system. However, the triple-extruder FEF machine cannot use the same methodology because all three syringes deliver material through a single orifice, and the back pressure caused by advancing one plunger will affect the forces acting on the other cylinders. Given the already complex and limited nature of the adaptive control technique [9] and taking into consideration the possibility of multiple materials with different viscosities being extruded simultaneously, force control was not a viable option. In order to alleviate this issue, a general tracking controller was developed to run the linear cylinders with desired (reference) velocities. The linear cylinder dynamics are modeled as

$$\tau \dot{v} + v = Ku - f \tag{1}$$

where τ is the time constant (s), v is the plunger speed (mm/s), K is the gain (mm/s/V), u is the control voltage (V), and f is the friction (mm/s). To determine the model parameters, i.e., τ, K, and f, a pyramid command voltage signal is sent to the servo motor and the corresponding plunger speed is recorded. The model parameters then are determined using a particle swarm optimization algorithm [14,15], which is an evolutionary computational technique based on swarm intelligence. In the particle swarm algorithm, the trajectory of each particle (i.e., set of candidate model parameters) in the search space is adjusted according to its own experience and the experience of the other particles in the swarm. The resulting model parameters are listed in Table 1. To demonstrate the model's performance, the simulated cylinder/plunger velocity using the developed model is compared with the measured velocity, as shown in Figure 4. The results demonstrate that the linear cylinder model fits the experimental data very well. A general tracking controller, as shown in Figure 5, is then designed to track the reference velocity v_r. The sampling period, T_s, is 0.01 s.

Table 1: Linear cylinder parameters

Cylinder	τ (s)	K (mm/s/V)	f (mm/s)
1	$3.60 \cdot 10^{-3}$	11.95	0.934
2	$4.82 \cdot 10^{-3}$	11.81	1.056
3	$4.26 \cdot 10^{-3}$	11.62	1.022
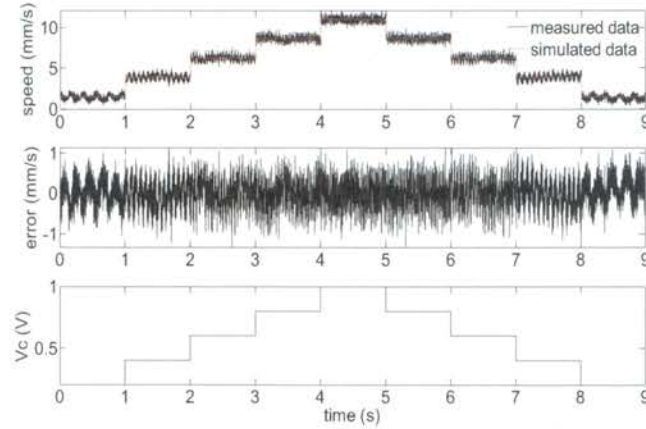
Figure 4: Comparison of the linear cylinder 1 velocity model and experimental results
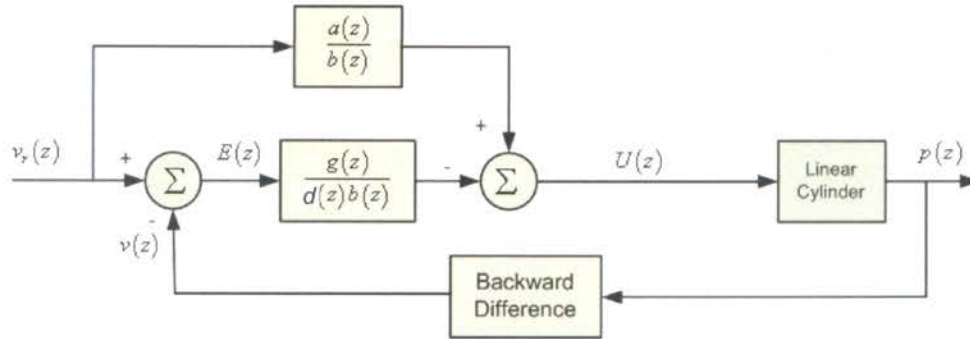
Figure 5: General tracking velocity controller

Here,

$$\frac{V(z)}{U(z)} = \frac{k\left(1-e^{-T/\tau}\right)}{z - e^{-T/\tau}} = \frac{b(z)}{a(z)} \tag{2}$$

and $d(z) = z-1$ in Figure 5 is the disturbance-generating polynomial. By including this polynomial, the Internal Model Principle is utilized to robustly reject constant

disturbances such as Coulomb friction. The characteristic polynomial $d(z)a(z)-g(z)$ is designed to have two poles located at $-e^{-Ts/\tau_1}$ and $-e^{-Ts/\tau_2}$; thus, the controller polynomial $g(z)$ is

$$g(z) = g_1(z) + g_0 = \left(e^{-T_s/\tau_1} + e^{-T_s/\tau_2} - 1 - e^{-T_s/\tau}\right)z + \left(e^{-T_s/\tau} - e^{-T_s/\tau_1 - T_s/\tau_2}\right) \qquad (3)$$

The control signal is

$$u(k) = u(k-1) + \frac{v_r(k+1) - \left(1 + e^{-T_s/\tau}\right)v_r(k)}{K\left(1 - e^{-T_s/\tau}\right)} + \frac{e^{-T_s/\tau}v_r(k-1) - g_1 e_v(k) - g_0 e_v(k-1)}{K\left(1 - e^{-T_s/\tau}\right)} \qquad (4)$$

where the speed error is

$$e_v(k) = v_r(k) - v(k) \qquad (5)$$

4.2. Analytical Determination of Transport Delay

The system transport delay must be repeatable and accurately predicted in order for the path planning algorithm to deposit material in the desired location. The transport delay of the system t (sec) was modeled using linear relationships between the paste volumetric flow rate Q (m³/sec) and the combined internal volume of each segment of the static mixer V (m³). Variations in the paste's viscosity and compressibility, as well as the effects of gravity, were considered negligible, thus, the volumetric flow rates of pastes can be related to the time delay for steady state flow as follows:

$$t = \frac{V}{\displaystyle\sum_{i=1}^{n} Q_i} \qquad (6)$$

where n represents the number of cylinders being used. For the triple-extruder system, equation 6 becomes:

$$t = \frac{V}{A_1 v_1 + A_2 v_2 + A_3 v_3} \qquad (7)$$

where A (m²) is the cross sectional area of the cylinder, and v (m/sec) is the plunger's velocity. The combined flow rate from all three extruders, Q, is equal to the sum of the individual flow rates, Q_1, Q_2 and Q_3. The ratio of $Q_1:Q_2:Q_3$ can be used to represent the ratio of the three pastes in the material composition. For example, to achieve a mixture of 50% each of paste one and paste two:

$$Q_1 : Q_2 : Q_3 = 0.5 : 0.5 : 0 \qquad (8)$$

With constant volume in the static mixer, increasing plunger velocity results in less time delay required to change materials. However, the extruded length of paste remains unchanged for the same nozzle orifice. Thus a better approach for paste mixing is to reduce the volume of the static mixer as long as complete mixing of the pastes can be achieved.

4.3. Experimental Verification of Analytical Transport Delay

Experiments were performed to verify the analytical transport delay by recording the time taken to switch the deposition from one material to another. For example, paste in the first barrel was extruded until the extrusion force reached a steady state value, at which point the velocity of the first plunger v_1 was set to zero, and the velocity of the second plunger v_2 was set to the reference velocity. A time delay measurement was taken from the point at which the material was switched to the point at which the material appeared to fully transition into the next material. This transition takes place in 60 to 200 seconds in our observations and it occurs because the second material being extruded must clear out the previous material from the internal surface of the static mixer. As the paste travels along the sidewalls and elements of the mixer, some degree of intermixing will occur before a complete change of material takes place. The time required to begin the transition to the time required to fully transition into the next material accounts for approximately 15 to 30% of the total time delay in our observations. The time required from the beginning of the transition to halfway through the transition when compared to the theoretical time delay calculated from equation 7 for four different plunger velocities is shown in Figure 6.
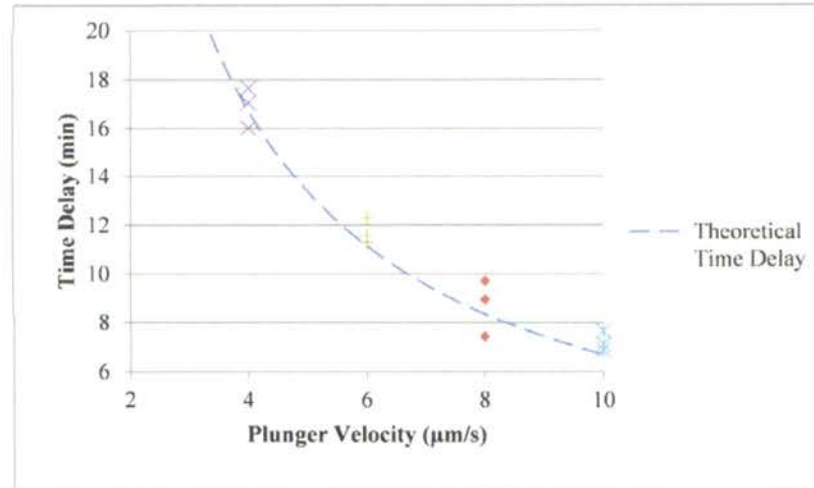
Figure 6: Experimental validation of the time delay model at four plunger velocities

The experimental results yield good accuracy for each plunger velocity when compared to the analytical predictions. For each velocity, the average of three runs comes within <4% of the theoretical time delay. One important factor in successful time delay repeatability is to ensure that the paste has been pre-loaded, or compressed, at the steady state force in each syringe prior to extrusion. For example, at a plunger velocity of 10 μm/s, the time delay averages seven minutes. When the target material was not pre-loaded to the steady state force (typically 600 N) prior to extrusion, delay times of up to fifteen minutes were observed. This increased delay has been thought to occur because the paste being used has some degree of compressibility which allows material from one syringe to enter the other if the two syringes are not both pre-loaded to an equal force. This compressibility also adds error to the time delay measurements if the paste is not pre-loaded, by introducing a transient phase to the initial startup as the force ramps up to a steady state value. For continuous extrusion, this issue can be solved by maintaining a steady extrusion force for both cylinders. However, planning of tool paths for extrusion on demand (EOD), as required for most motion code programs must take this compressibility into account to avoid lengthening the time delay and facing the consequence of materials switching at an undesired location.

5. CONTROL OF MATERIAL GRADIENTS

The algorithm developed to control the material gradient has two main functions: 1) implementing compensation for material transport delay and 2) applying material composition gradients to existing tool path motion code for homogeneous materials. The cylinder shown in Figure 7 was built by manually changing the velocity of each plunger to achieve a gradient from green to pink limestone ($CaCO_3$) paste in increments of 10% composition. In this case, G-code was written manually using circular arc functions, and the time delay was calculated and tested manually by varying the velocity of each plunger. The composition was varied by 10% every ten layers from the bottom (green) to the top

Figure 7: Cylinder with vertical gradient

(pink). It can be observed that composition increments near 10% for this height achieve a nearly continuous gradient over short distances from one material to the next. The goal of the gradient control algorithm is to automate this process for any geometry. In order to make the algorithm more versatile, it was designed to take in tool path information from both the Stratasys Insight software and generic G&M code to apply the transport delay and material gradients. With this functionality, primitive shapes such as plate or bar test specimens can be coded manually in G&M code and loaded into the program to apply the gradient and transport delay without having to model these simple shapes and go through the slicing and conversion process.

5.1. Program Overview

The program was written in Mathworks Matlab 8, and its operation is outlined in Figure 8. It first reads in a text file output from Stratasys Insight, which includes tool path information in the format of Categorical Abstract Machine Language (CAML). Because motion control is executed through Delta Tau PEWIN software, tool path information must be translated into G&M coding language. Commands such as table speed (feed rate), extrusion status (on/off), and motion commands in the absolute positioning domain are extracted and converted. The resulting code is then modified to include Extrusion on Demand (EOD) commands and varying composition gradients by

controlling the speed of each servo motor. With each incremental change in position, a corresponding distance traveled is associated with each set of two points. This distance is appended into an array and its cumulative distance is monitored to determine the current location within the 3D part being built. Lastly, changes in composition are modified to occur earlier by a factor determined by the time delay. This delay is expressed in the length of the material extruded as determined by multiplying the time delay t (sec) by the desired table speed s (m/sec). The cumulative distance array is used to index the location of the gradient switch, and the new position within the code at which the change in velocity must take place is based on the transport delay. If the velocity must change before executing the motion code (e.g., if the composition is being changed near the beginning of a part), a DWELL command is sent to the controller to first carry out a purge cycle until the motion code can be run to achieve the desired gradient.

Insight Software   Matlab file conversion

| Import STL file to path planning software; export tool path file | Read in tool path information | Convert tool path code into G&M code for PMAC | Code for extrusion on demand (EOD) |
| Load file into FEF machine | Output tool path with transport delay and gradient information as G&M code | Implement transport delay for changes in cylinder velocity | Apply material composition gradient based on user input |

Figure 8: Schematic for Matlab program to apply multiple material compositions to the existing tool path code

5.2. Gradient Control Algorithm

Following the conversion to G&M code, the resulting tool path information is inserted into a matrix that includes the feed rate, M-code commands, coordinate information (X,Y,Z), incremental distance between each pair of coordinate points, the current layer, and any G-code commands. The feedrate is used to determine the time required for any necessary dwell commands. Coordinate information with corresponding distances and layers is used directly for the gradient control algorithm. All other parameters are simply passed through to be output to the final code. The primary transformation that takes place applies composition gradients in a user-defined

orientation and increment (Figure 9) to the existing code. The first step in this process is to determine at what time to vary the velocity of each ram in order to achieve the desired gradient. The algorithm reads in each row to first acquire the cumulative distance traveled up to that point (CD). This is achieved by adding the incremental distance (D) from the previously calculated tool path matrix to the current distance. At the end of each layer the layer number (L_i) and length of extrudate on the current layer (CL_i) are output to a layer information matrix used by the gradient algorithm.

User input is required to first identify whether the gradient is to occur in the vertical or horizontal direction, which is used for raster path generated parts. In addition, a composition increment (ΔC) needs to be defined as a percentage of paste A to paste B (e.g., assuming even distributions, a composition increment of 25% would indicate that the part be split into five sections, with a composition of 0%B, 25%B, 50%B, 75%B and 100%B, respectively, from the beginning of the extrusion path to the end in the direction of the raster path).

Determination of vertical gradients is based on the total number of layers in a part (L_{total}). After being split into sections (ΔL) the tool path matrix is once again referenced within a loop and outputs a true case only if the current layer is divisible by the ΔL (e.g., if the composition changes every six layers, $\Delta L=6$ and rem($L/\Delta L$) will equal 0 for layers 6, 12, ...). If true, the distance required to switch materials (D_n) is calculated by taking the current cumulative distance (CD) and subtracting a transport delay (D_{delay}) for the current gradient (G_n). These values are output to a matrix referenced in a final transformation to apply motor velocity changes with an applied transport delay.

User Defined gradient → Composition increment(ΔC) (e.g., 25%)

Import layer info. Matrix [L_i CL_i] ← Vertical — Vertical or Horizontal? — Horizontal → Import layer info. Matrix [L_i CL_i]

for L=i:L_{total}

$\Delta L = L_{total} * \Delta C$

rem(L/ΔL)? !=0, read next layer

==0 Apply transport delay

$D_n = CD - D_{delay}$

[$D_0 G_0$; $D_n G_n$] — Output matrix

for L=i:L_{total}

Calculate how often composition changes each layer

$\Delta D = CL_i * \Delta C$

Apply transport delay

$D_n = D_{n-1} + \Delta D - D_{delay} + CD$

[$D_0 G_0$; $D_n G_n$] — Output matrix

OR

Search original tool path cell matrix and insert cylinder velocity switch at distance D_n based on the desired gradient G_n

Figure 9: Gradient control algorithm schematic, where L=layer, D=distance, CD=cumulative distance, G=material gradient composition, CL=current layer, and D_{delay}=transport delay in terms of extruded length

5.3. Gradient Control Program Implementation

5.3.1. G-code Interpretation for Horizontal Gradients.
Single-layer horizontal raster patterns were written in G-code to be 10.16 cm in width and 12.7 cm in length with a raster width of 1.27 mm. The same motion code was processed by the gradient control algorithm for three trials of grey-colored alumina paste (material A) to uncolored white alumina (material B) to switch compositions every 4.23 cm from 100%A to 100%B with a mixture of 50%(A+B) in the middle. The change in composition is marked by a region of transitional mixing (7.5 to 10 mm) and then there is a full switch to the desired ratio. This transition occurs over the span of 6 to 8 lines and accounts for 60.9 to 81.3 cm of extruded length at 6.35 mm/s table speed. Each test performed similarly with each composition change occurring within 42 cm of extruded length from the desired point of switching as seen in Figure 10.

To test the ability of the gradient control algorithm to plan composition changes for multiple layers, a 2.54 cm by 10 cm test bar was modeled using 3D CAD software and the final tool path code was tested with the FEF machine. Figure 11 shows the eighth

layer of the test bar (4 mm in height), where the base layer is composed of 100% paste A and each subsequent layer contains a region to the right of 100% A (pink) and a region to the left of 100% B (green). Horizontal gradients showed repeatability from layer to layer within 1 cm in either direction for a total of eight layers. As mentioned previously, the transition region makes up 15-30% of the total time delay; therefore one limitation of the inline static mixer is a required minimal length for each layer in order to be able to fully transition from one material to the next. On average, for a plunger velocity of 10 μm/s, transitional mixing has been observed to take place in 81 cm or less. Since the overall length for each layer shown in Figure 11 is 203 cm, and 40% of the time extruding material is spent transitioning between paste A and paste B, only 30% of the part is pure A and 30% is pure B. This effect is undesirable for small parts, but larger parts may see some benefit from this transitional zone. For example, if two pastes composed of materials with different shrinkage rates are used to build a part, this transitional mixing will act as a buffer between composition changes to reduce the risk of delamination during the freeze-drying and sintering stages of post-processing. The pre-defined gradient could obviously be tailored such that drastic composition changes are avoided, but transitional mixing may add another level of protection to the green part and such complicated gradient schemes would not be necessary.
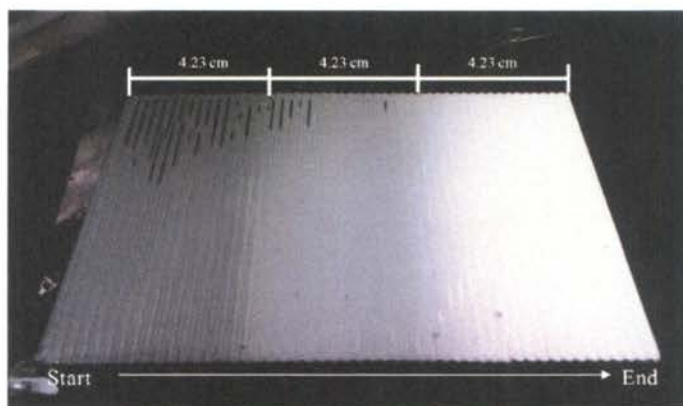
Figure 10: Transition from Al_2O_3 (gray) to Al_2O_3 (white), including a 50% mixing
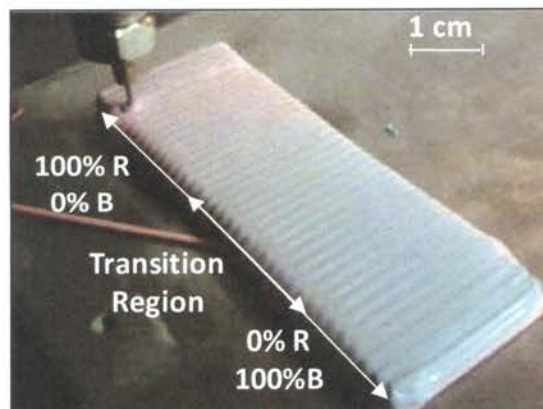
Figure 11: Eight-layer 2.54 cm by 10 cm block as the test bar.

5.3.2. G-code interpretation for Vertical Gradients. The vertical test bar shown in Figure 12 was produced using two pastes: 100% Alumina (paste A) and 50%Alumina-50%Zirconia (paste B). These tests were conducted to ensure the resulting mixture of paste A and paste B was of the correct composition. This part was built in an environment of -10°C from manually written G-code and automatically generated velocity control to vary the composition from 100% paste A
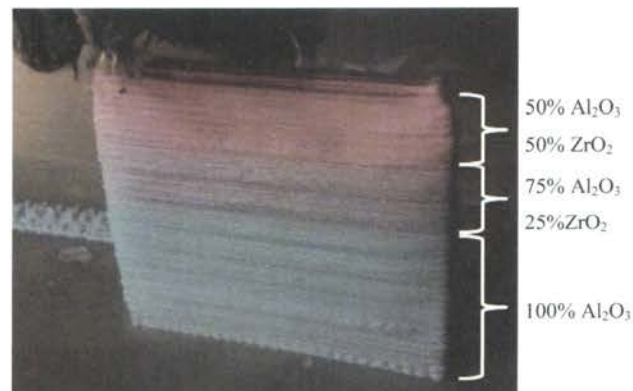
Figure 12: Alumina/Zirconia composite test part.

(100%Al_2O_3) for the first 20 layers to 50% paste A and 50% of paste B (75%Al_2O_3-25%ZrO_2) for the next 10 layers and 100% paste B (50%Al_2O_3-50%ZrO_2) for the final 10 layers. The part was freeze dried, sintered, cut and polished before applying a gold/palladium coating to condition the part for energy dispersive x-ray spectroscopy (EDS) measurements. Control pellets were manually mixed in precise measurements from the same alumina and alumina/zirconia pastes and sintered for comparison to the 75%Al_2O_3-25%ZrO_2 mixture to ensure the correct composition was being achieved. EDS intensity measurements verified that the mixture of the two pastes mixed and

deposited using the FEF process matched this composition from the control set by comparing the ratio of aluminum and zirconium from both sets of data.

6. CONCLUSIONS

A machine code generation algorithm has been developed to implement a material transport delay and apply heterogeneous material compositions to existing G&M code for additive manufacturing of multiple materials using a triple-extruder Freeze-form Extrusion Fabrication (FEF) system. The generated motion code has been verified by depositing single- and multiple-layer horizontal gradients and multiple-layer vertical gradients. The transport delay caused by the use of an inline static mixer was taken into account by analytical methods and verified with empirical data and observation. Future work will include the expansion of gradient control such as radial gradients and coordinate-specific gradients, using all three extruders of the FEF system. Various process parameters will be optimized for the FEF machine for use with functionally graded parts. The sintering behavior of graded parts will be investigated, and the materials and mechanical properties of densified FGM parts will be tested to evaluate the effectiveness of the process.

7. ACKNOWLEDGEMENTS

8. REFERENCES

[1] X. Kou and S. Tan, "A Hierarchical Representation for Heterogeneous Object Modeling," Computer-Aided Design, Vol. 37, pp. 307-319, 2005.

[2] A. Xu and L. Shaw, "SFF-Oriented Modeling and Process Planning of Functionally Graded Materials using a Novel Equal Distance Offset Approach," Proceedings of Solid Freeform Symposium , Austin, TX, pp. 544-552, 2004.

[3] T. Jackson, N. Patrikalakis, E. Sachs and M. Cima, "Modeling and Designing Components with Locally Controlled Composition," Proceedings of Solid Freeform Symposium, Austin, TX, pp. 259-266, 1998.

[4] U.S. Pat. No. 5738817, April 14, 1998.

[5] J. Cesarano III, R. Segalmen, and P. Calvert, "Robocasting Provides Moldless Fabrication from Slurry Deposition," Ceramics Industry, Vol. 148, pp. 94-102, 1998.

[6] E. Malone and H. Lipson, "Fab@Home: the Personal Desktop Fabricator Kit," Rapid Prototyping Journal, Vol. 13, No. 4, pp. 245-255, 2007.

[7] X. Zhao, "Experimental Investigation of Effect of Environmental Temperature on Freeze-form Extrusion Fabrication," Thesis, Missouri University of Science and Technology, Rolla, MO, 2007.

[8] T. Oakes, P. Kulkarni, R. Landers, and M. Leu, "Development of Extrusion-on-Demand for Freeze-form Extrusion Fabrication Processes," Proceedings of the 3rd Annual ISC Research Symposium, Rolla, MO, 2009.

[9] Zhao, X., Landers, R.G., and Leu, M.C., 2010, "Adaptive Extrusion Force Control of Freeze–form Extrusion Fabrication Processes," ASME Journal of Manufacturing Science and Engineering, Vol. 132, No. 6, 064504.

[10] Mason, M.S., Huang, T., Landers, R.G., Leu, M.C., and Hilmas, G.E., "Aqueous–Based Extrusion of High Solids Loading Ceramic Pastes: Process Modeling and Control," Journal of Materials Processing Technology, Vol. 209, No. 6, pp. 2946–2957, 2009.

[11] M. Mason, T. Huang, M. Leu, R. Landers and G. Hilmas, "Aqueous-Based Extrusion Fabrication of Ceramics on Demand," Eighteenth Annual Solid Freeform Fabrication Symposium, Austin, TX, 2007.

[12] T. Huang, M. Mason, G. Hilmas, and M. Leu, "Aqueous Based Freeze-form Extrusion Fabrication of Alumina Components," Rapid Prototyping Journal, Vol. 15, No. 2, pp. 88-95, 2009.

[13] T. Huang, M. Mason, G. Hilmas, and M. Leu, "Freeze-form Extrusion Fabrication of Ceramic Parts," International Journal of Virtual and Physical Prototyping, Vol. 1, No. 2, pp. 93-100, 2006.

[14] J. Kennedy and R.C. Eberhart, "Particle Swarm Optimization," IEEE International Conference on Neural Networks, Perth, Australia, November 27–December 1, pp. 1942–1948, 1995.

[15] L. Tang, J. Ruan, R. Landers., and F. Liou, "Variable Powder Flow Rate Control in Laser Metal Deposition Processes," ASME Journal Manufacturing Science and Engineering, Vol. 130, No. 4, pp. 041016, 2008.

PAPER II

Hybrid Extrusion Force-Velocity Control Using Freeze-form Extrusion Fabrication for Functionally Graded Material Parts

Bradley K. Deuser, Lie Tang, Robert G. Landers, Ming C. Leu, and Greg E. Hilmas

Department of Mechanical and Aerospace Engineering

Missouri University of Science and Technology, Rolla, Missouri 65409

Abstract

Freeze-form Extrusion Fabrication (FEF) is an additive manufacturing process that uses an aqueous-based paste loaded with ceramic or metal powder to build complex three-dimensional (3D) parts by extruding the material from a syringe onto a solid substrate in a sub-zero temperature environment. An intelligent control methodology for paste extrusion is developed in this paper that utilizes a hybrid extrusion force-velocity controller. A plunger velocity controller is used to ensure steady extrusion flow rate and an extrusion force controller is developed to precisely regulate the start and stop of extrusion. Both controllers are coupled with a hybrid control scheme for extrusion on demand and air bubble release compensation. The plunger velocity controller successfully regulates the output material composition from two syringes and the extrusion force controller is able to precisely control the extrusion start and stop. Air bubble release compensation reduces the severity of gap defects and extrusion track thinning resulting from air bubble release. Monolithic and functionally graded parts are fabricated to illustrate the functionality of the hybrid extrusion force-velocity controller.

1. INTRODUCTION

Functionally Graded Material (FGM) part fabrication refers to the process of building parts with multiple materials in a graded fashion in order to take advantage of complementary material properties while minimizing residual stresses from the sintering process [1]. Ceramic parts are often used in high-temperature applications for their

superior heat resistance. However, they are difficult to manufacture as geometrically complex composites using traditional processes. Several additive manufacturing technologies have been developed in recent years that can fabricate complex geometry ceramic components; however, few have the capability to build FGM parts.

Additive manufacturing (AM) technology is capable of fabricating complex three-dimensional (3D) geometry parts additively in a layer-by-layer fashion using polymers, metals, and ceramics. Widely used AM processes in industry such as Stereolithography [2], Fused Deposition Modeling [3], 3D printing [4], and Selective Laser Sintering (SLS) [5] began as polymer-based methods; however, several of these processes have evolved to include the ability to fabricate metal and ceramic parts. Most metal and ceramic-based technologies, such as SLS [6], are limited to single material (monolithic) part fabrication since they use a powder bed. Robocasting [7], Extrusion Freeform Fabrication [8], Shape Deposition Manufacturing [9], and Laser Metal Deposition [10] are better suited to build multiple-material parts since they are deposition-based processes.

Freeze-form Extrusion Fabrication is capable of building 3D parts by depositing aqueous-based pastes loaded with ceramic or metal powder in a layer-by-layer manner. Fabrication is conducted with a specially-designed machine in a sub-zero temperature environment to freeze the paste quickly after deposition, thus minimizing the amount of organic binder necessary. This results in easier and more environmentally friendly post-processing [11-15]. This machine is equipped with a triple-extruder mechanism to build complex geometry FGM parts.

One of the challenging aspects of extrusion-based freeform fabrication is the ability to start and stop extrusion on demand. The FEF process uses ceramic or metal aqueous-based colloidal pastes with typical solids loading of 45-50% by volume. Degassing of the ceramic or metal pastes via high-shear vacuum mixing minimizes the amount of air entrapped within the paste; however, some degree of compressibility is still present. An analytical process model derived from first principles by Li et al. [16] explains this behavior. In order to have reliable control of extrusion on demand an extrusion force controller is developed using this model and measured extrusion force feedback to account for inconsistency in the amount of air in the paste. By directly controlling the applied force to the plunger, the output extrusion rate is regulated.

This study uses Freeze-form Extrusion Fabrication (FEF) to fabricate FGM parts using a hybrid extrusion force-velocity control scheme. Our previous research validated the use of an extrusion force controller for regulating the extrudate velocity and for start and stop extrusion on demand for a single-extruder system [17]. The multiple-extruder machine in this study uses a hydraulic manifold to combine two or three pastes into a single inline static mixer before the mixture is deposited onto a solid substrate. This coupling is necessary for mixing, but results in hydraulic interference between the extrusion forces applied to each syringe and allows one paste to flow into another cylinder. As a result, extrusion force control alone cannot be used to regulate the flow rate of each paste; rather, it is used to increase the extrudate speed of response for starting and stopping extrusion on demand while plunger velocity control is used to regulate the steady-state flow rate of each paste. Both controllers are utilized in a hybrid control scheme to have intelligent control of extrusion on demand. In addition, hybrid control is used to compensate for air bubble release, which typically results in gap defects and extrusion track thinning.

2. FREEZE-FORM EXTRUSION FABRICATION PROCESS OVERVIEW

The FEF machine is equipped with three servo controlled extruders and an inline static mixing unit to combine the pastes through a single orifice (Figure 1). The paste is then deposited onto a build platform using a nozzle heated to just above the freezing point of water.
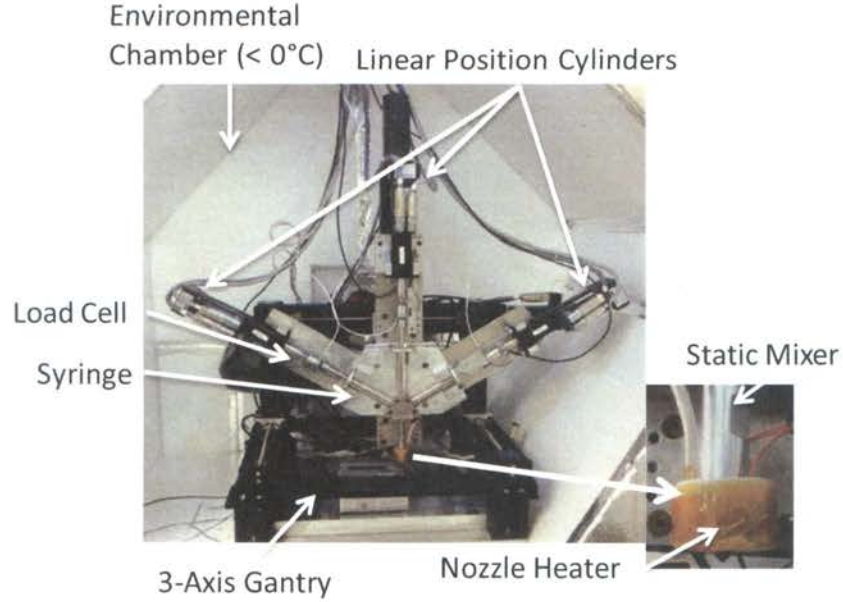
Figure 1: FEF System Setup.

This mixing technique blends together multiple pastes into a homogeneous mixture; however, it introduces a transport delay into the system, denoted t_d. The transport delay is modeled using linear relationships between the paste volumetric flow rate Q (mm^3/s) and the internal volume of the static mixer V (mm^3) as follows:

$$t_d = \frac{V}{\sum_{i=1}^{n} Q_i} = \frac{V}{A_1 v_1 + A_2 v_2 + A_3 v_3} \tag{1}$$

where $n = 3$ is the number of cylinders being used, A_i is the cross sectional area of the ith cylinder (mm^2), and v_i is the velocity of the ith plunger (mm/s). The volumetric flow rate from all three extruders, Q, is equal to the sum of the flow rates from the individual cylinders, Q_1, Q_2, and Q_3. The ratio of these three flow rates represents the ratio of the three pastes; therefore, the composition ratio is controlled by regulating the velocity of each plunger, as illustrated in Figure 2.
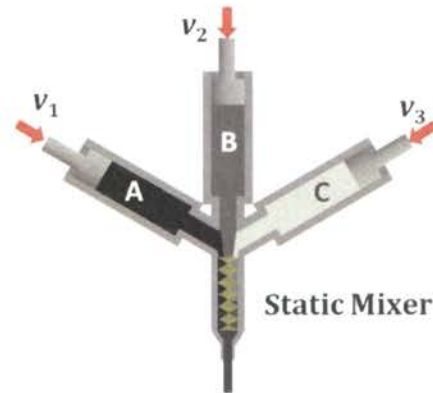
FGM Green Part

Figure 2: Triple extruder mechanism for static mixing of up to three colloidal pastes to form an FGM part.

The FEF system is comprised of two coupled mechatronic systems (Figure 3). Extrusion is controlled with three Kollmorgen servo motors (N2 Series AKM23D) using a Servostar300 series amplifier and a National Instruments PXI chassis with LabVIEW Real Time. Each servo motor drives a linear position cylinder and the encoders are sampled by a counter/timer card (PXI-6602) run in quadrature mode, and a first order finite difference scheme is utilized to achieve a velocity resolution of 0.2 μm/s. Each linear cylinder is equipped with a load cell (Omega LC-305) to track the amount of force being exerted on a stainless steel plunger, which is housed in a stainless steel syringe. The load cells have a maximum load rating of 4448 N and a resolution of 7 N. The load cell signals are sampled through a PXI-6025E multifunction card with an A/D resolution of 12 bits at a maximum sampling rate of 200 kS/s and an input range of ± 10 V. Command voltages are sent to the servo motor amplifiers through a PXI-6711 high-speed analog output card, which has a 12-bit D/A resolution, a maximum sampling rate of 1MS/s and a voltage range of ± 10 V.

The three-axis gantry system is controlled using a Delta Tau Turbo PMAC card, which operates the FEF machine through NC G&M motion code via PEWIN 32 software. The two systems are coupled by sending analog signals from the Delta Tau system to the PXI-6025E LabVIEW multifunction board and an A/D converter.
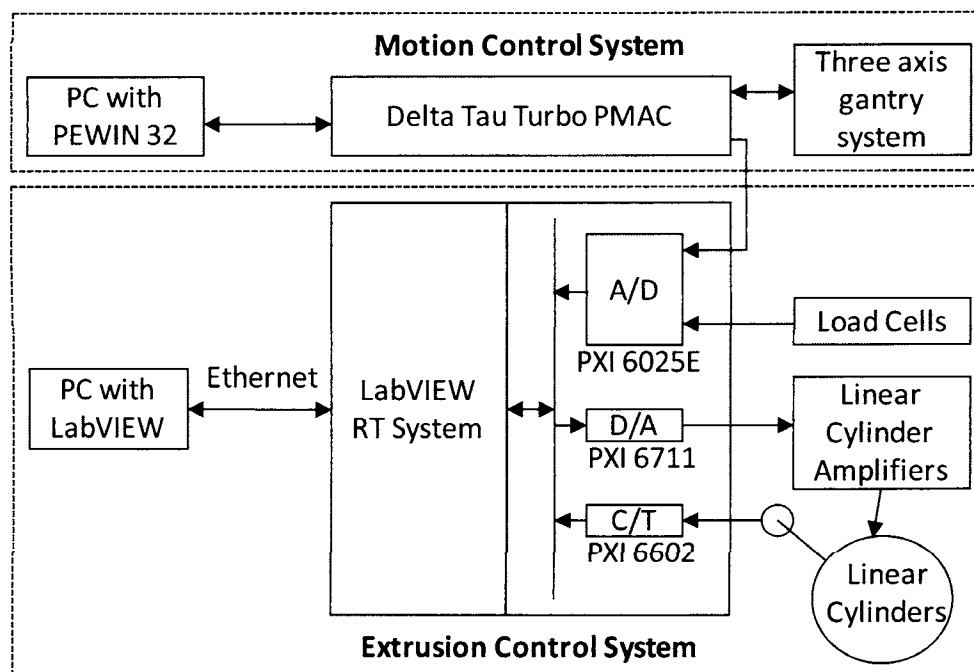
Figure 3: FEF system schematic for extrusion and motion control.

Deposition of colloidal pastes has several challenges; however, the most fundamental ones are 1) regulation of the steady-state extrusion speed for each of the multiple extruders and 2) the ability to start and stop extrusion on demand. By controlling the velocity of each plunger, the individual flow rate of each paste can regulate the output composition. This plunger velocity controller is used to regulate the individual velocities from each syringe in addition to the velocity of the paste exiting the nozzle (i.e., the extrudate velocity) after it has reached a steady-state value. However, the plunger velocity controller cannot be used to regulate extrusion on demand due to paste compressibility, which causes a slow transient response for starting and stopping extrusion - three orders of magnitude slower than using an extrusion force controller.

An extrusion force controller is developed in this paper to intelligently regulate extrusion on demand by directly controlling the amount of force applied to the plunger. If the force applied to the plunger is decreased below a critical shear rate, extrusion will cease. The extrusion force directly correlates to the output extrudate velocity; therefore, regulating the extrusion force regulates the output flow rate faster than the plunger velocity controller and thus can be used to control extrusion on demand.

Both the plunger velocity controller and extrusion force controller have unique benefits; therefore, a hybrid control scheme is developed to utilize the two controllers to take advantage of the ability to control the output flow rate from multiple syringes with the plunger velocity controller and increase the speed of response for extrusion on demand with the extrusion force controller. This hybrid extrusion force-velocity controller is also used to compensate for the release of air bubbles, which may cause large void defects in a part. Extrusion force control has been observed to quickly correct for air bubble release. This is achieved by switching the control scheme to extrusion force control when air bubble release occurs while the velocity controller is active.

3. PLUNGER VELOCITY MODELING AND CONTROL

Each servo motor drives a linear cylinder, which advances the plunger at a rate determined by the applied voltage. Plunger velocity controllers are used to regulate the individual flow rates from each syringe by using model-based feedback controllers.

3.1. Linear Servo Motor Model

The servo-driven extruder system is modeled for a no load case (i.e., no extrusion) by a first order linear differential equation relating the plunger velocity u_p (mm/s) to the command voltage V_c (V)

$$\tau_u \dot{u}_p(t) + u_p(t) = K_u V_c(t) - f_u \, \text{sgn}(u_p) \tag{2}$$

where τ_u is the time constant (s), K_u is the gain (mm/s/V), and f_u is the Coulomb friction magnitude (mm/s). To determine these unknown model parameters, a pyramid command voltage from 0 to 1 V is sent to the servo motor and the corresponding plunger velocity is recorded (Figure 4). The model parameters are determined using a Particle Swarm Optimization algorithm [18]. The resulting model parameters are listed in Table 1. To validate the model of linear cylinder 1, the plunger velocity was simulated and compared with the measured plunger velocity as shown in Figure 4. The results demonstrate that linear cylinder 1 model fits the experimental data within ±1 mm/s. Similar results are achieved for the other two linear cylinders. The modeling error is caused by using a first order finite backward difference method to calculate the plunger velocity from the

measured position data and uncertanties such as stiction and Stribeck friction effects, which cause stick-slip at lower velocities [19].
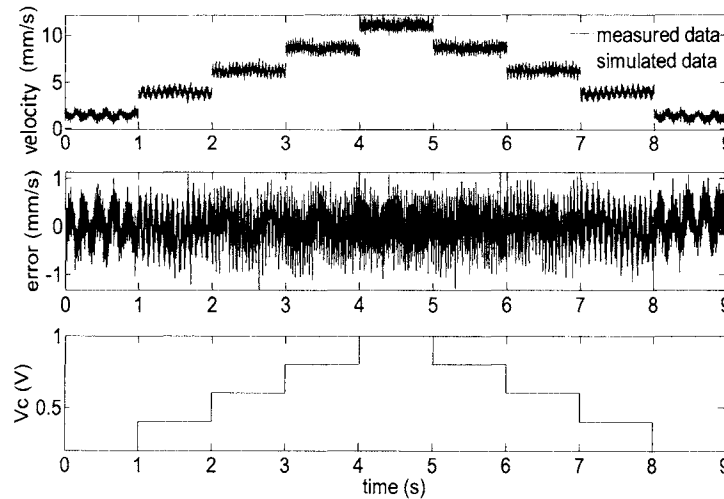
Figure 4: Linear cylinder 1 velocity model and experimental results.

Table 1: Linear cylinder model parameters.

Cylinder	τ_u (ms)	K_u (mm/s/V)	f_u (mm/s)
1	3.60	11.9	0.934
2	4.82	11.8	1.06
3	4.26	11.6	1.02

The extrudate velocity cannot be directly sensed in real in the present FEF system; therefore, it is controlled in open-loop using a plunger velocity controller. The steady-state extrudate velocity is proportional to the plunger velocity by the conservation of mass flow rate. The variability of the open-loop plunger velocity is ±1 mm/s as shown in Figure 4; therefore, a feedback controller is developed in order to achieve higher resolution of the steady-state plunger velocity. The minimum plunger velocity is 1 μm/s due to the resolution of the servo motors and the maximum velocity is limited by the resulting extrusion force and servo motor capacity (1000 N). Since the system is hydraulically coupled between syringes, each servo motor experiences the same extrusion force; therefore, the sum of the individual plunger velocities is limited to 10 μm/s for the

paste used in this study to achieve extrusion forces near 60-80% of the servo motor capacity. This plunger velocity range satisfies composition ratios as high as 9:1 for a two-paste system.

3.2. Plunger Velocity Controller

A general tracking controller, shown in Figure 5, is designed to track the reference velocity of each linear cylinder. The sampling period is $T_s = 10$ ms.
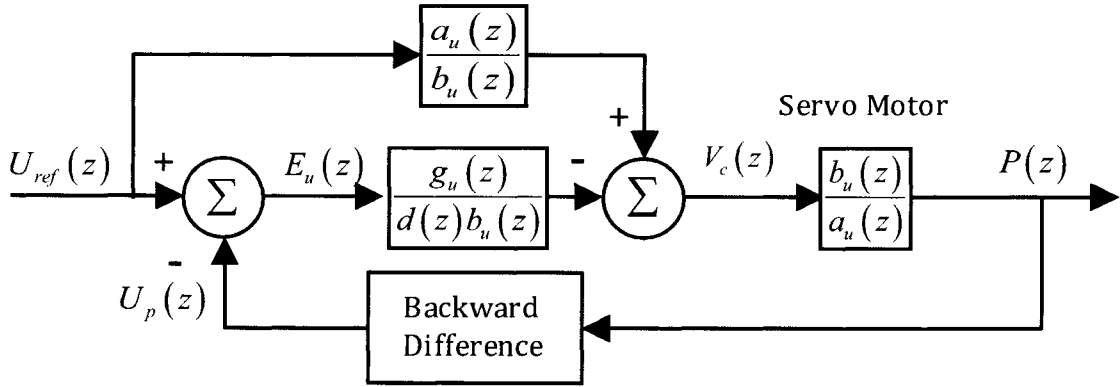
Figure 5: General tracking velocity controller block diagram.

The linear cylinder transfer function in the Z domain, ignoring Coulomb friction and using a Zero Order Hold, is

$$\frac{U_p(z)}{V_c(z)} = \frac{K_u\left(1 - e^{-T_s/\tau_u}\right)}{z - e^{-T_s/\tau_u}} = \frac{b_u(z)}{a_u(z)} \tag{3}$$

The term $d(z) = z - 1$ in Figure 5 is the disturbance-generating polynomial. By including this polynomial, the Internal Model Principle is utilized to robustly reject constant disturbances, such as Coulomb friction, and track constant references. The characteristic polynomial $d(z)a_u(z) - g_u(z)$ is designed to have two poles located at $-e^{-T_s/\tau_1}$ and $-e^{-T_s/\tau_2}$, where τ_1 and τ_2 are the desired closed loop time constants, which are selected to be on the same order of magnitude as the motor time constants and are 5 and 5.1 ms, respectively. The controller polynomial $g_u(z)$ is

$$g_u(z) = g_1 z + g_0 = \left(e^{-T_s/\tau_1} + e^{-T_s/\tau_2} - 1 - e^{-T_s/\tau_u}\right)z + \left(e^{-T_s/\tau_u} - e^{-T_s/\tau_1 - T_s/\tau_2}\right) \tag{4}$$

The control signal is

$$V_c(k) = V_c(k-1) + \frac{u_{ref}(k+1) - \left(1 + \dot{e}^{-T_s/\tau_u}\right)u_{ref}(k) - e^{-T_s/\tau_u}u_{ref}(k-1)}{K_u\left(1 - e^{-T_s/\tau_u}\right)} - \frac{g_1 e_u(k) + g_0 e_u(k-1)}{K_u\left(1 - e^{-T_s/\tau_u}\right)} \qquad (5)$$

where u_{ref} (mm/s) is the reference plunger velocity and the plunger velocity error is

$$e_u(k) = u_{ref}(k) - u_p(k) \qquad (6)$$

The general tracking plunger velocity controller is tested using a reference plunger velocity pyramid step input from 2 to 10 μm/s (Figure 6). The noise observed in this figure is from two sources: 1) operating near the minimum velocity range of the linear cylinders (1 μm/s) and 2) using a first order backward finite difference method to estimate the plunger velocity. The steady-state error is approximately ±2 μm/s after filtering the data using a first order low-pass filter with a cut-off frequency of 40 Hz.

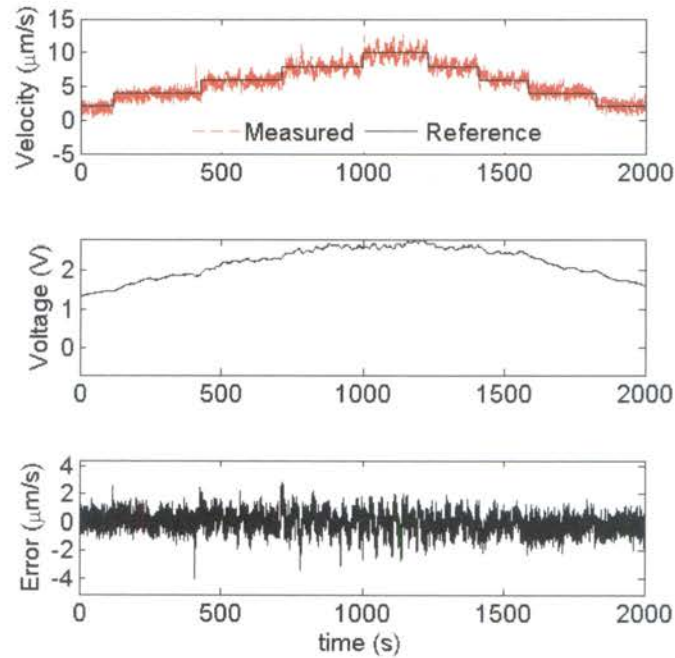Figure 6: Plunger velocity controller response to a pyramid step input reference velocity trajectory.

4. EXTRUSION FORCE MODELING AND CONTROL

Since the extrusion force is directly correlated to the steady-state and transient behavior of the extrudate velocity, an extrusion force controller is developed to compensate for the slow extrudate velocity response to changes in plunger velocity. Fast

response is primarily needed for starting and stopping extrusion on demand; however, extrusion force control can also be used to recover from anomalies such as the release of air bubbles, which may cause large defects in the part to occur when using plunger velocity control due to the slower extrudate velocity response.

4.1. Dynamic Extrusion Force Modeling

The dynamic extrusion force model developed by Li et al. [17] is

$$\frac{df_L(t)}{dt} = \frac{\left(f_L(t) - f_f + A_p p_{atm}\right)^2}{A_p p_0 l_0}\left[u_p(t) - u_a(t)\right]\cdot 10^{-3} \tag{7}$$

Where f_L (N) is the extrusion force, f_f (N) is the friction force between the paste and barrel, A_p (m³) is the plunger cross sectional area, p_0 (Pa) is the initial pressure in the syringe, and l_0 (m) is an effective air layer thickness. This "air layer" represents an effective entrapped volume of air within the paste that causes the paste to behave as a compressible fluid. The variable u_a (mm/s) describes the steady-state velocity achieved at a given extrusion force, which is a function of paste rheology and is

$$u_a(t) = \left(\frac{f_L(t) + \alpha}{\beta}\right)^\varepsilon \tag{8}$$

where α, β, and ε are model parameters. This empirical relationship is determined by commanding a plunger velocity pyramid step input from 2–10 μm/s and measuring the steady-state extrusion force. For an aqueous-based aluminum oxide (Al_2O_3) paste with a solids loading of 45% by volume, the power-law model parameters are determined to be $\alpha = -46.3$, $\beta = 1950$, and $\varepsilon = 3.20$, and the modeled goodness of fit is 0.9974. The measured and modeled steady-state extrusion forces are shown in Figure 7.
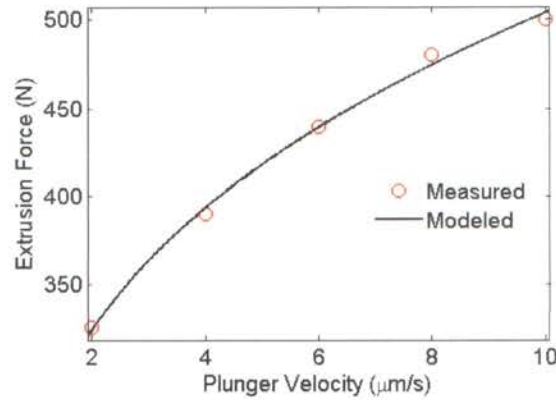
Figure 7: Measured and modeled steady-state extrusion forces.

The dynamic extrusion force model is simulated with a step input plunger velocity of 4 to 10 µm/s and compared to the measured extrusion force in Figure 8. The volume of air within the paste is impractical to measure for each batch of paste; therefore, the volume of air is estimated based on empirical data by observing the difference between the measured and simulated dynamic extrusion force responses and adjusting the estimated volume of air such that the simulation and experimental results match for the first step in plunger velocity. The results match for the first step in plunger velocity when the approximate air volume is 1.4% of the total volume of paste within the syringe (i.e., an air layer thickness of 0.9 mm). The initial pressure within the syringe p_0 is calculated from the initial measured extrusion force. At 218 Pa, this "preload" represents the initial pressure of the paste within the syringe and the minimum pressure required to completely fill the nozzle and initiate extrusion. The simulation's initial conditions are matched to the initial conditions of the experiment.

For the simulation in Figure 8, the extrusion force model resulted in modeling errors within ±20 N, which is approximately three times that of the load cell resolution. An exception is the drop in force at 720 s, which can be attributed to an air bubble release. The open-loop time constant decreases from 56 s to 22 s as the plunger velocity increases 2 to 10 µm/s and the extrusion force increases from 330 to 500 N. The time constant then gradually increases to 59 s as the plunger velocity is reduced from 10 to 2 µm/s.
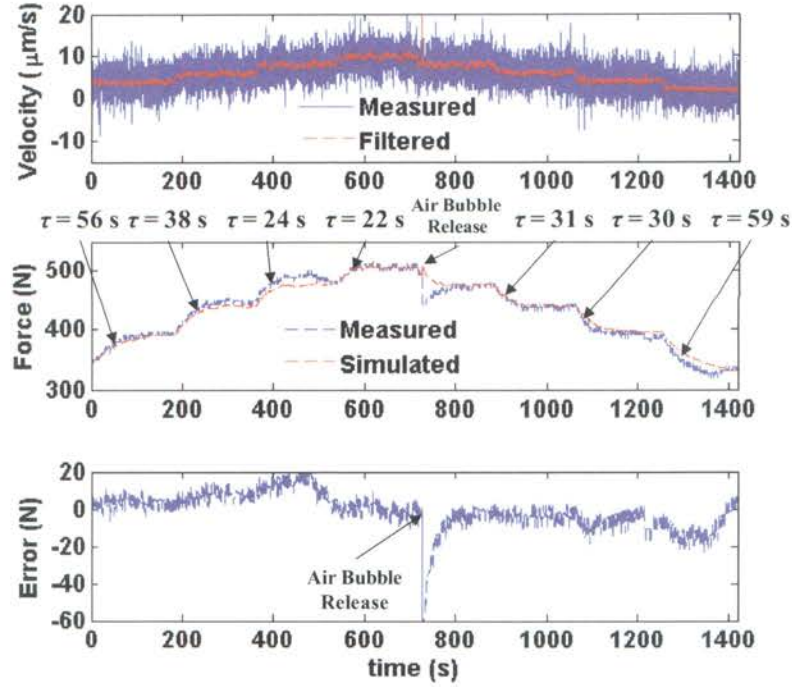
Figure 8: Simulated and measured extrusion forces for $p_0 = 218$ Pa and $l_0 = 0.9$ mm. An air bubble release occurs at 720 s.

4.2. Dynamic Extrusion Force Model Linearization

In order to have robust tracking of the extrusion force, a linearized model-based feedback controller is implemented. The nonlinear model presented in Equation 7 is linearized as follows:

$$g = \dot{f}_L(t) \approx g\left(\overline{f}_L, \overline{u}_p, t\right) + a\left[u_p(t) - \overline{u}_p\right] + b\left[f_L(t) - \overline{f}_L\right] \tag{9}$$

$$a = \left.\frac{\partial g}{\partial f_L}\right|_{\overline{u}_p, \overline{f}_L} = \frac{\left(\overline{f}_L - f_f + A_p P_{atm}\right)^2}{A_p P_0 l_0}\left[-\frac{\varepsilon}{\beta}\left(\frac{\overline{f}_L + \alpha}{\beta}\right)^{\varepsilon-1} \cdot 10^{-6}\right] \tag{10}$$

$$b = \left.\frac{\partial g}{\partial u_p}\right|_{\overline{u}_p, \overline{f}_L} = \frac{\left(\overline{f}_L - f_f + A_p P_{atm}\right)^2}{A_p P_0 l_0} \tag{11}$$

where $\overline{f}_L$ is the nominal extrusion force (N) and $\overline{u}_p$ is the nominal plunger velocity (m/s). The incremental linearized model is

$$\tau_L \dot{\hat{f}}_L(t) + \hat{f}_L(t) = K_L \hat{u}_p(t) \tag{12}$$

where $\tau_L = 1/a$ is the linearized time constant (s) and $K_L = b/a$ is the linearized plunger velocity coefficient (N/(mm/s)). The incremental extrusion force (N) and plunger velocity (mm/s), respectively, are

$$\hat{f}_L(t) = f_L(t) - \overline{f}_L \tag{13}$$

$$\hat{u}_p(t) = u_p(t) - \overline{u}_p \tag{14}$$

The linearized system time constant and plunger velocity coefficient are functions of the nominal extrusion force. As the plunger velocity approaches zero, the linearized time constant and plunger velocity coefficient approach infinity and the extrusion force approaches a constant value, which is 46 N in this case (Equation 7). This limit represents the minimum extrusion force required to initiate extrusion for the alumina paste used in this study. Below this critical extrusion force threshold, extrusion will cease because the shear rate is not sufficient to initiate extrusion. As the plunger velocity and extrusion force increase, the linearized time constant approaches zero as the paste behaves more like an incompressible fluid due to the reduction in the compressible volume of the air within the paste (Figure 9).
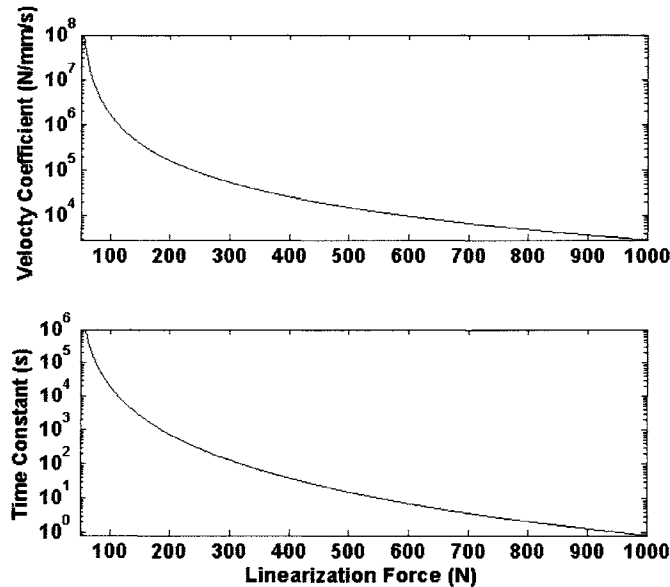

Figure 9: Linearized extrusion force model open-loop time constant and plunger velocity coefficient with respect to nominal extrusion force.

4.3. Extrusion Force Controller

A general tracking controller is designed based on the linearized extrusion force model. The controller block diagram is shown in Figure 10. The plunger velocity control system is ignored as its response time is much smaller than that of the closed-loop extrusion force control system.

The incremental extrusion force process transfer function is

$$\frac{\hat{F}_L(z)}{\hat{U}_p(z)} = \frac{K_L\left(1-e^{-T_s/\tau_L}\right)}{z-e^{-T_s/\tau_L}} = \frac{b_f(z)}{a_f(z)} \tag{15}$$

Similar to the velocity controller, the characteristic polynomial is designed to have two poles located at $-e^{-T_s/\tau_{1f}}$ and $-e^{-T_s/\tau_{2f}}$. The extrusion force response should be as fast as possible without resulting in system instability; therefore, the minimum time constant is empirically determined to be 200 ms, and the second time constant is selected to be 400 ms. This results in an overdamped response with a controller time constant of approximately 400 ms. The controller polynomial is

$$g_f(z) = g_{1f}z + g_{0f} = \left(e^{-T_s/\tau_{1f}} + e^{-T_s/\tau_{2f}} - 1 - e^{-T_s/\tau_L}\right)z + \left(e^{-T_s/\tau_L} - e^{-T_s/\tau_{1f}-T_s/\tau_{2f}}\right) \tag{16}$$

The general tracking extrusion force control signal is

$$\hat{U}_p(k) = \hat{U}_p(k-1) + \frac{\hat{F}_{ref}(k+1) - \left(1+e^{-T_s/\tau_L}\right)\hat{F}_{ref}(k) - e^{-T_s/\tau_L}\hat{F}_{ref}(k-1)}{K_L\left(1-e^{-T_s/\tau_L}\right)}$$
$$-\frac{g_{1f}\hat{e}_f(k) + g_{0f}\hat{e}_f(k-1)}{K_L\left(1-e^{-T_s/\tau_L}\right)} \tag{17}$$

where $\hat{F}_{ref} = F_{ref} - \overline{f}_L$ is the incremental reference extrusion force (N), F_{ref} is the reference extrusion force (N), and the extrusion force error is

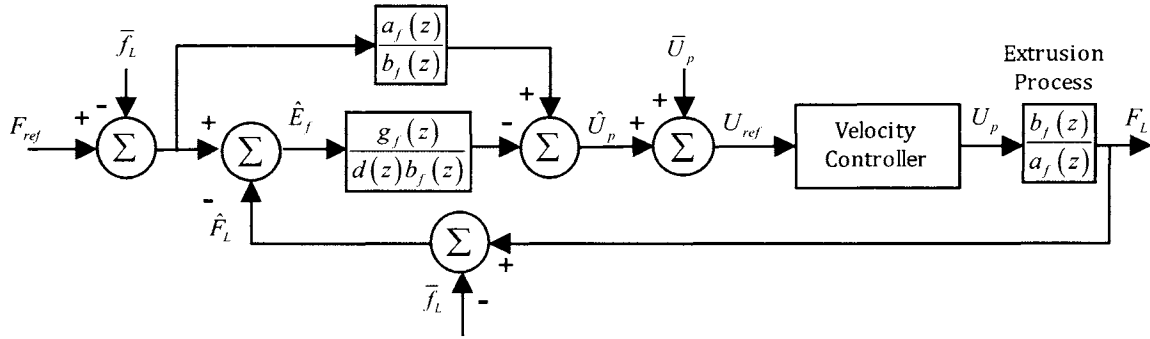$$\hat{e}_f(k) = F_{ref}(k) - F_L(k) \tag{18}$$

Figure 10: Linearized general tracking force controller block diagram.

The general tracking extrusion force controller is experimentally implemented for a series of constant reference extrusion forces and the results are shown in Figure 11. The results illustrate that the controller is successful in reducing the open-loop time constant of 59 s to the desired closed-loop time constant of 0.4 s for a positive change in reference extrusion force and a time constant of 0.2 s for a negative change in extrusion force reference. This difference between positive and negative changes in the extrusion force can be attributed to two factors: 1) neither the extrusion force model or the plunger velocity model take negative velocities into account; therefore, this uncertainty will cause deviation in the expected time constant and 2) there is unmodeled nonlinear behavior in the plunger velocity as the voltage passes through zero from positive to negative that is largely due to un-modeled friction effects. These factors can also cause the paste in the linear cylinder to lose contact with the plunger. The steady-state error is on the order of ±10 N, which is comparable to the resolution of the load cells (7 N). The extrusion force controller operates by rapidly accelerating the plunger to compresses the paste in the syringe. Large oscillations are observed during the first step that can be attributed to the fact that the paste was not initially compressed. The commanded plunger velocity is near zero and potentially negative as it attempts to regulate the extrusion force near the critical extrusion force. As the extrusion force is reduced from 500 to 100 N, the entrapped air within the paste retains some compression and the oscillations are not seen.
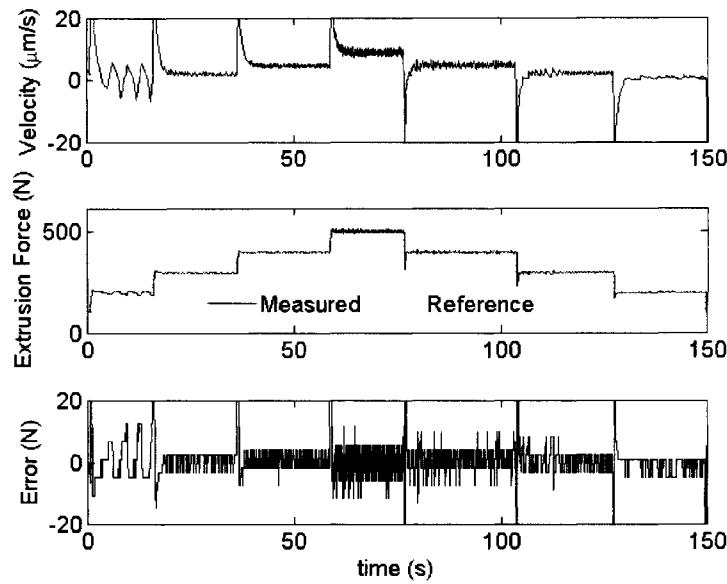
Figure 11: Extrusion force general tracking controller experimental results.

5. HYBRID CONTROL

The hybrid extrusion force-velocity controller determines when to switch between the extrusion force and plunger velocity controllers. It is used for extrusion on demand and compensating for air bubble release in FGM part fabrication. The Delta Tau motion system uses G-code to control the 3-axis gantry positioning of the tool head, and it communicates with the National Instruments real-time system to issue "start" and "stop" extrusion commands as the G-code activates system variables that are interfaced with the LabVIEW system. Air bubble release compensation is conducted by monitoring the measured extrusion force while operating in plunger velocity control mode, and switching to extrusion force control mode if the system detects an air bubble release.

5.1. Extrusion on Demand

Extrusion on demand is necessary for complex part fabrication because it is not feasible for any tool path planning software to generate tool paths with purely continuous extrusion profiles. Short tool path segments may be present based on part geometry, and each layer typically contains several segments (i.e., loops) that require extrusion to begin and end at the terminal points in the segment. Therefore, an extrusion-on-demand

controller must have a rapid response in order to have the ability to deposit short segments with acceptable quality as well as limit part build times.

The motion system "start" and "stop" extrusion commands by setting the corresponding internal system variable to either ON or OFF. Extrusion is initiated after the deposition nozzle reaches its desired location by setting this variable ON. Following this command, the extrusion force controller activates and sets the reference extrusion force to a predetermined value to reach the desired plunger velocity. Once activated, each plunger advances to compress its paste until the desired extrusion force is achieved. A timer is set to switch back to plunger velocity control mode after the settling time of the extrusion force controller (1.6 s in the present study). Limiting the amount of time in extrusion force control mode ensures the flow rate of individual syringes is maintained.

Plunger velocity control is used for the majority of the part build time. When the motion system encounters a "stop" command, the internal system variable is set to OFF, the timer is reset for the next "start" command, and the extrusion force controller is activated with a reference value of 50 N to cease extrusion and maintain a preload on the syringe. If the reference extrusion force value is set too low (< 20 N) the controller becomes unstable; however, if the extrusion force is set too high, extrusion will not stop entirely. The instability is due to the fact that the load cell loses contact with the plunger if it attempts to reduce the extrusion force past a threshold near the resolution of the load cells (~7 N). Each plunger will maintain preload on the syringe until the next "start" command is issued.

Figure 12 demonstrates the response of the extrusion force controller as the Delta Tau system issues a "start" command, noted by a positive change in extrusion force, and a "stop" command, noted by a negative change in extrusion force. For a steady-state plunger velocity of 10 μm/s, the required extrusion force is 500 N; therefore, the reference extrusion force is set to 500 N when a "Start" command is issued. The system responds with a 1.6 s settling time for positive changes in extrusion force and a settling time of 0.8 s for negative changes in extrusion force associated with "Stop" commands.
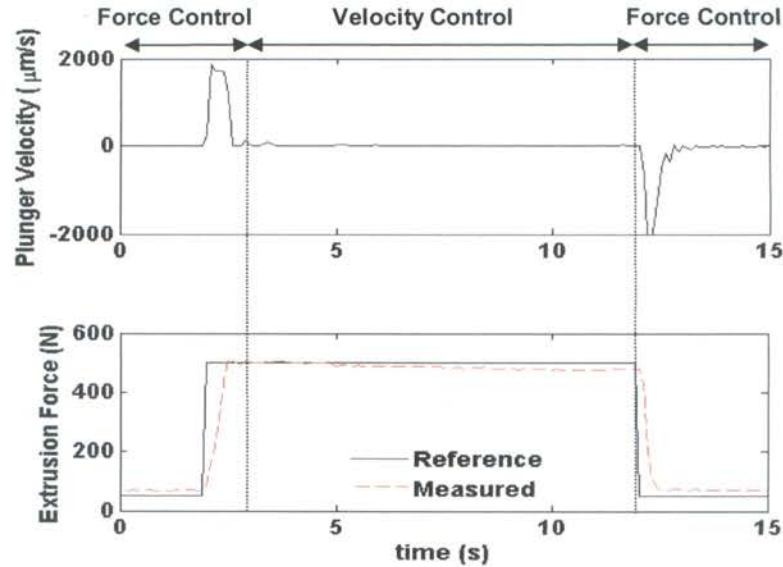
Figure 12: Plunger velocity and extrusion force responses for step change in extrusion force reference from 50 to 500 N to start extrusion and from 500 to 50 N to stop extrusion.

5.2. Dwell-Based Start and Stop Method

Extrusion on demand using a dwell-based method works by positioning the extrusion nozzle at the desired start or stop location and pausing motion for a certain amount of time after issuing a "start" or "stop" command before proceeding to the next motion command. The dwell-based method is investigated by depositing a series of three 12.7 mm paths (Figure 13). Upon receiving a command to start extrusion, the controller is given a step reference extrusion force of 500 N and dwells for a set amount of time (100 to 600 ms) before depositing each segment. Once commanded to stop, the controller sets the reference extrusion force to 50 N and dwells for 100 to 600 ms (Figure 13a). The stop dwell time is assessed by similarly dwelling at the end of each extrusion line before moving to the next line (Figure 13b). This figure shows that it is feasible to use the dwell method for "start" commands since the extrudate track width remained visually consistent, with no thinning or excessive build up of the paste. The optimal dwell time was between 400 and 500 ms. Stop dwell is ineffective because paste continues to exit the nozzle for approximately 100 ms after the command is issued and

causes material to build up. Therefore, a trajectory-based method is investigated to cease extrusion before the end of a segment.
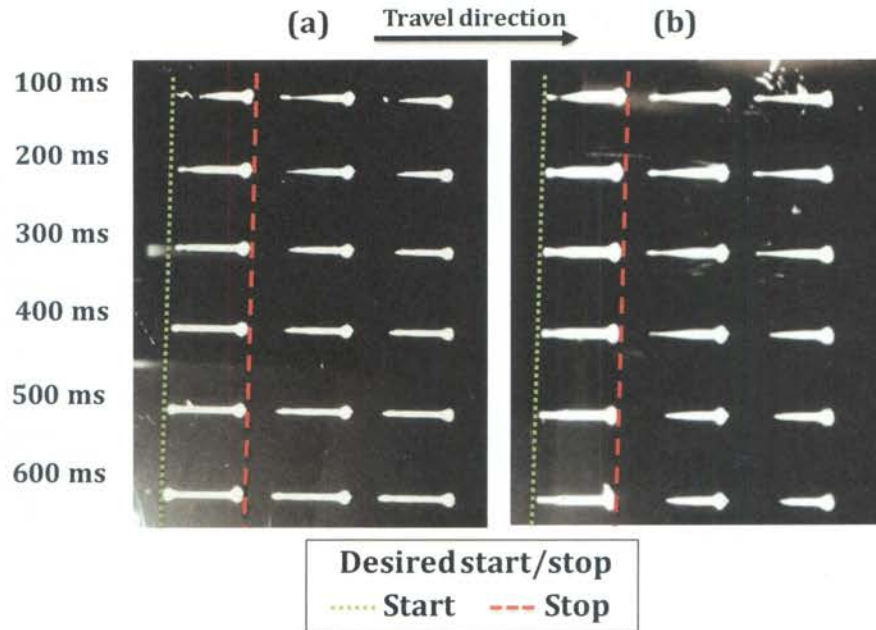

Figure 13: Extrusion segment deposition using the dwell-based method. (a) Dwell start from 100 to 600 ms at the beginning of each segment with 200 ms stop dwell and (b) Dwell stop from 100 to 600 ms at the end of each segment with 200 ms start dwell.

5.3. Trajectory-Based Start and Stop Method

The trajectory-based method issues a "start" or "stop" command to the extruder before the desired start or stop point. This method is tested for start commands by initiating extrusion from 100 to 400 ms before the initial segment point is reached (Figure 14a) and for stop commands by retracting the plunger from 20 to 100 ms before the final segment point is reached (Figure 14b). Trajectory start serves as a validation for the delay time, which is 400 ms for both trajectory and dwell-based start methods. Trajectory stop is capable of producing a constant extrusion track width, with no excessive build-up. Approximately 20 to 40 ms is required to stop extrusion. Longer delay times cause the extrudate track to stop short before the end of the segment, whereas shorter delay times cause build up at the end of the segments.
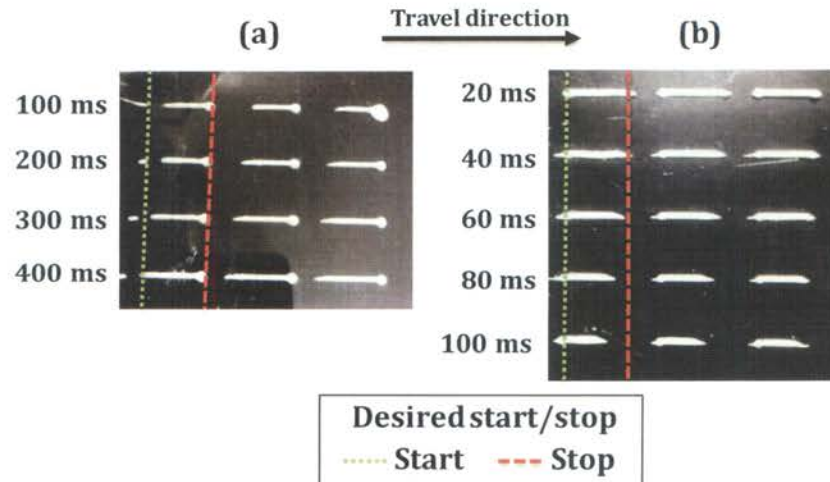
Figure 14: Extrusion segment deposition using trajectory-based method. (a) Early start from 100 to 400 ms ahead of time with 400 ms stop dwell and (b) Early stop from 20 to 100 ms ahead of time with 400 ms start dwell.

5.4. Air Bubble Release Compensation

An added benefit of using a hybrid force-velocity controller is the ability to minimize defects caused by the release of an entrapped air bubble during part fabrication. This capability is evaluated by injecting an air bubble (approximately 1 ml) into the paste. A serpentine pattern is deposited onto a solid substrate until air bubble release occurs. If a velocity controller is utilized, the recovery period after the air bubble releases exhibits a slow first order response, as illustrated in Figure 15a. This causes a sudden spike in the velocity, caused by rapid depressurization, a jump in the plunger position, and a sudden drop in the extrusion force. In this case, the drop in the extrusion force is 50 N and it takes approximately 18 s to reach the original extrusion force since the reference plunger velocity remains constant. During this time, a large gap defect occurs in the deposited material as seen in Figure 16a. The extrusion force controller can minimize gaps formed from air bubble release by adjusting the reference plunger velocity to maintain a constant force on the plunger (Figure 15b). Increasing the reference plunger velocity compensates for the volume lost to the expansion of the air bubble, resulting in a much shorter gap defect as seen in Figure 16b.
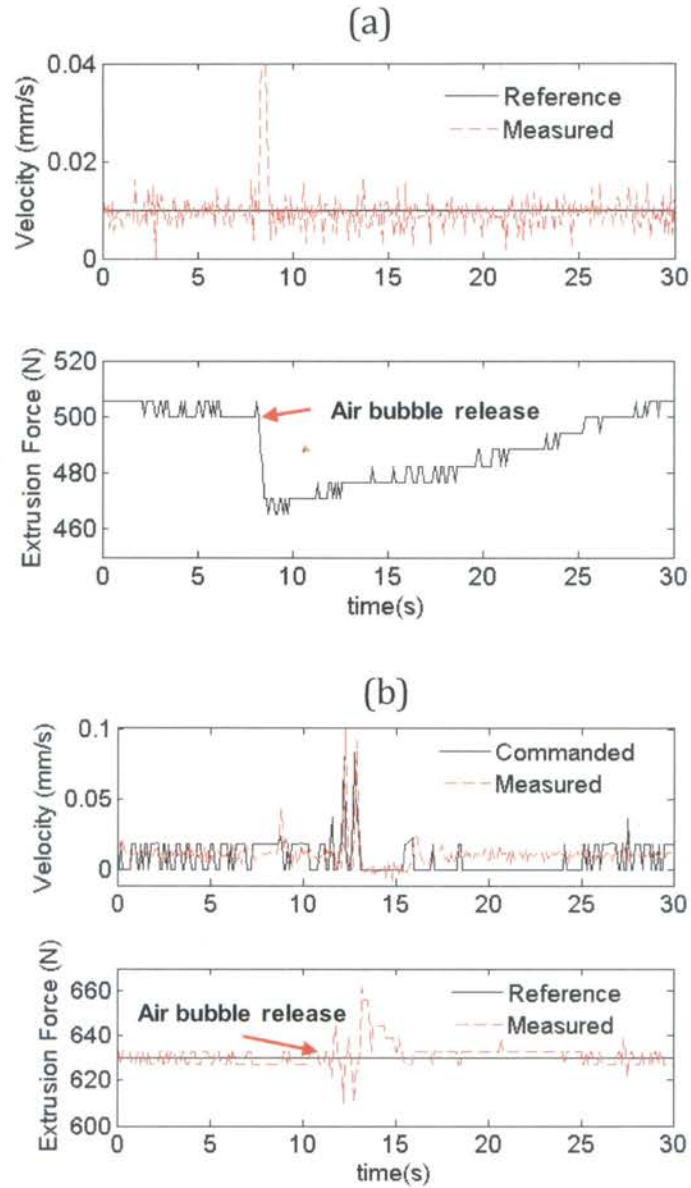
Figure 15: Experimental plunger velocity and extrusion force responses to an air bubble release for (a) velocity controller with $u_{ref} = 0.01$ mm/s and (b) extrusion force controller with $F_{ref} = 630$ N.
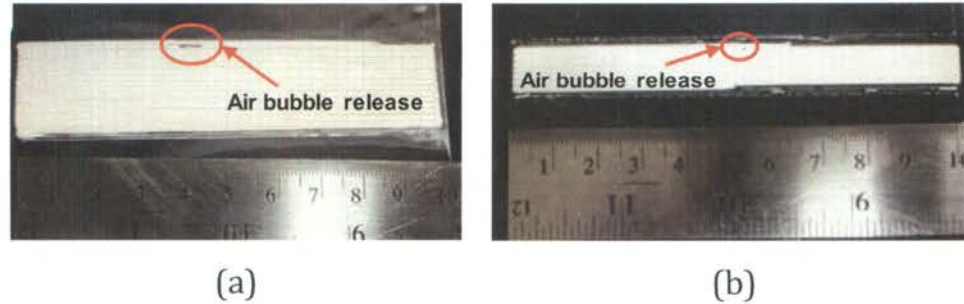
(a)   (b)

Figure 16: Parts with gap defects caused by an air bubble release for (a) velocity controller with u_{ref} = 0.01 mm/s and (b) extrusion force controller with F_{ref} = 630 N.

Following an air bubble release, the output flow rate is reduced when using the plunger velocity controller, which may result in a gap defect or a thin extrusion track width until the extrusion force rises back to the steady-state extrusion force. Both cases can be seen in Figure 17a. Gap defects of 2-4 mm are observed and a thinned track width follows one air bubble release, affecting 60 mm of extrudate length. The extrusion force controller responds within 100 ms and the resulting defect is less than 0.5 mm in length, nearly undetectable after the subsequent track fills in a major portion of the gap (Figure 17b).

(a)   (b)
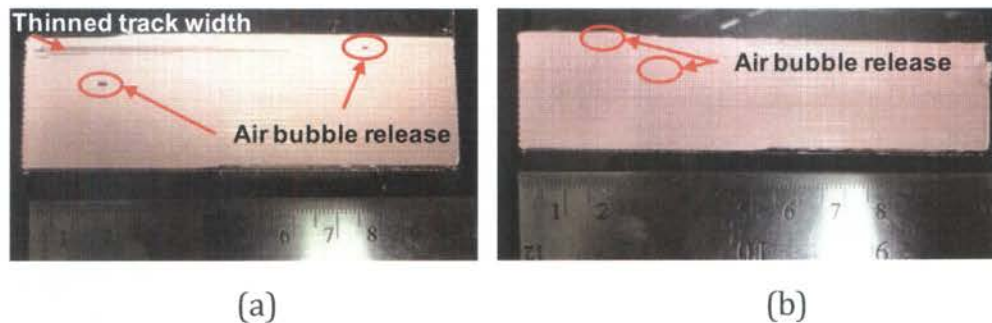
Figure 17: Parts with defects due to air bubble release using (a) velocity controller with u_{ref} = 0.01 mm/s and (b) extrusion force controller with F_{ref} = 630 N.

The hybrid force-velocity controller discussed is implemented to account for air bubbles by using a conditional control structure. Plunger velocity control is used continually for steady-state extrusion to regulate the flow rate of each syringe; however, if the measured force drops to more than 20 N below the reference extrusion force, the

control scheme switches to extrusion force control to regulate the extrusion force until the extrusion force is again within 20 N of the reference extrusion force, at which point plunger velocity control is re-enabled. This method allows the output flow rate to be quickly corrected within 400 ms (i.e., the closed-loop time constant of the extrusion force controller) following an air bubble release. Figure 18 demonstrates the use of this hybrid controller in the presence of an air bubble release. A serpentine pattern is deposited using the plunger velocity controller after injecting approximately 1 ml of air into the system. An air bubble release is encountered at 1.8 s, which causes a drop in the measured extrusion force past the 20 N threshold. After the extrusion force controller activates, only 0.2 s is required to fully recover since the reference plunger velocity is accelerated from 10 µm/s during steady-state to a maximum of 300 µm/s as the extrusion force controller adjusts the plunger velocity to maintain the reference extrusion force value. The table speed in this experiment is 12.7 mm/s and the air bubble release causes the extrusion force controller to activate within 200 ms. During this delay time, a 2.5 mm gap defect occurs due to the sudden loss of pressure within the syringe.
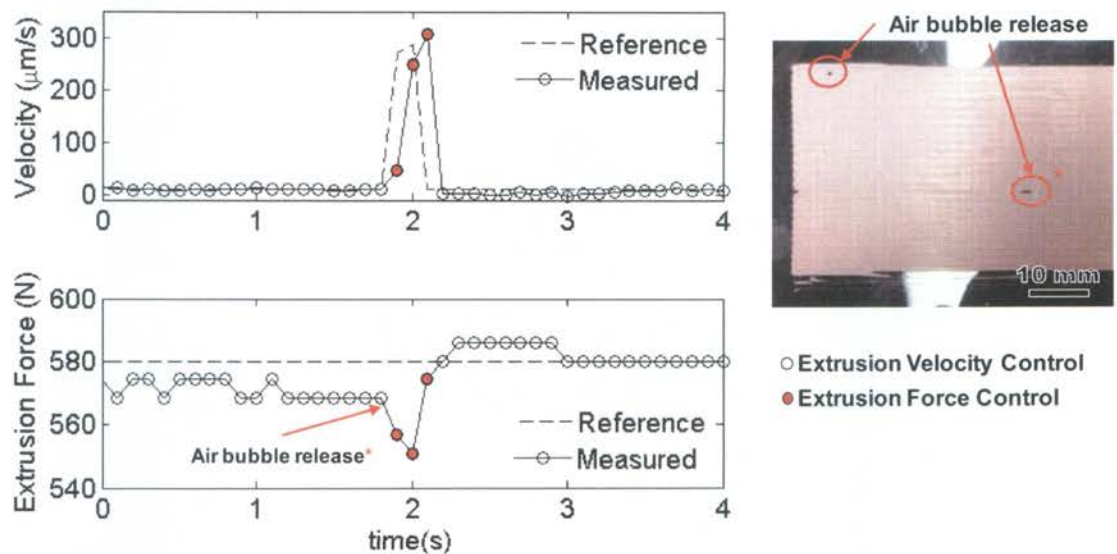

Figure 18: Measured extrusion force and plunger velocity for air bubble release when using the hybrid force-velocity controller.

The ability of the controller to use plunger velocity control is critical for fabrication of functionally graded parts since the flow rate of each material is regulated via the velocity of each plunger. The switching scheme described allows extrusion force control to be utilized for an instant following an air bubble release to correct the pressure within the syringe and regain the proper flow rate. Without air bubble release compensation (i.e., plunger velocity control alone), an entire part could be ruined if an air bubble release occurs during fabrication. While the hybrid force-velocity controller is not a substitute for proper paste preparation and loading techniques, it will minimize the defects associated with air bubble release during part fabrication.

6. DEMONSTRATION AND IMPLEMENTATION

The effectiveness of the hybrid controller was tested using an open-source tool path planning program, Skeinforge, to fabricate monolithic and functionally graded material parts. The files of tool paths generated by this path planning software were modified such that the FEF machine could interpret the tool path files (Figure 19). Process parameters such as extrudate bead width, standoff distance, and table velocity are determined through experimentation with the FEF machine. Extrusion-on-demand is regulated using the dwell-based start method (400 ms dwell) and the trajectory-based stop method (20 ms ahead of the stop point).
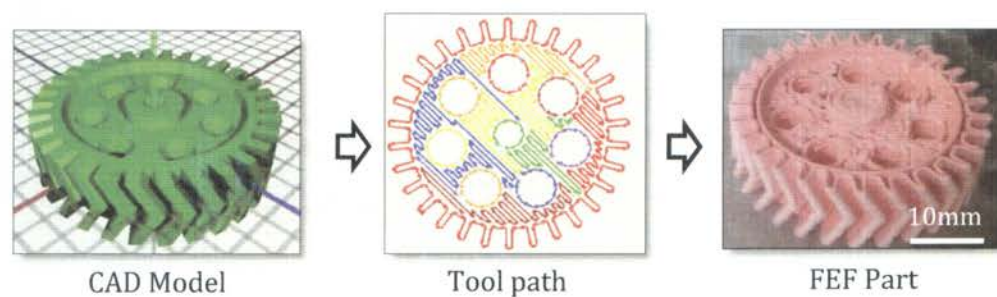

CAD Model   Tool path   FEF Part

Figure 19: Tool path generation flow chart for FEF part fabrication.

Single material parts are fabricated using alumina (Al_2O_3) paste in a freezing environment (-10°C) to demonstrate the ability of the hybrid controller to start and stop extrusion on demand for parts of complex shapes (Figure 20). Slope features as much as

45° from the vertical axis can be fabricated with no support structure, and the extrusion-on-demand control scheme allows the FEF machine to fabricate parts of varying size and complexity. The hybrid controller successfully switches between extrusion force control and plunger velocity control to maintain consistent extrusion width and no gaps in the tool path due to improper starting/stopping or due to air bubble release are observed during part fabrication.
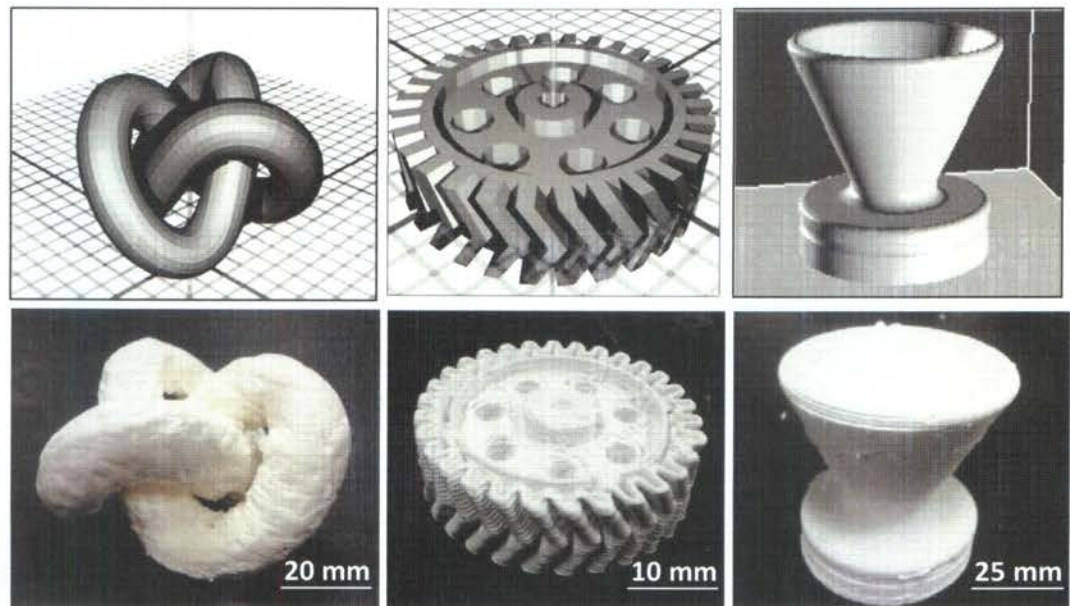
Figure 20: Sample parts made with Al_2O_3 paste.

Fabrication of functionally graded parts using the developed hybrid control scheme was demonstrated by fabricating a three-composition part (100% paste 'A', 50% paste 'A' and 50% paste 'B', 100% paste 'B') using two calcium carbonate ($CaCO_3$) pastes of pink and blue colors to represent two different materials (Figure 21). Three 3D models were created in a CAD software package to represent three compositions of paste 'A' and paste 'B'. The tool path was generated for each component and a splicing program combined the tool paths into a single one with variable plunger velocities to account for multiple materials. The transport delay model was incorporated to account for change of compositions by shifting the reference plunger velocities ahead by the calculated transport delay. Paste compositions were successfully regulated from 100% paste 'A' to 100% paste 'B' using the plunger velocity controller for two syringes, and

the extrusion force controller was utilized for start and stop commands in the tool path. The part is built on a layer-by-layer basis to form a radial gradient from the inner hemispherical region (paste 'A') to the outer block region (paste 'B') with a composition of 50% paste 'A' and paste 'B' between the two pure compositions.
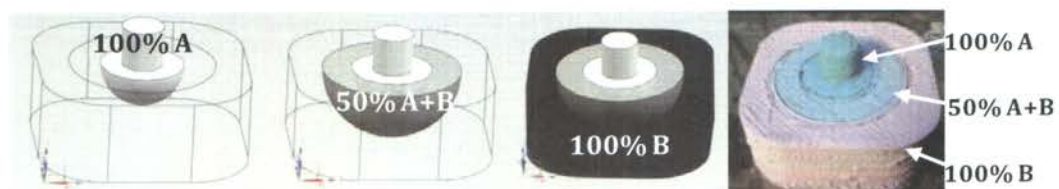

Figure 21: Demonstration of fabricating a functionally graded material part using two CaCO$_3$ pastes of pink and blue colors.

7. SUMMARY AND CONCLUSIONS

A hybrid force-velocity controller has been developed to regulate the steady-state extrusion flow rate using a plunger velocity controller and to regulate extrusion-on-demand using an extrusion force controller for fabricating functionally graded material parts using the freeze-form extrusion fabrication process. Plunger velocity control is used normally for steady-state extrusion to regulate the flow rate of each syringe; however, the control scheme switches to extrusion force control when the measured force drops by more than a certain amount below the reference extrusion force. Extrusion force control is used in order to control extrudate start and stop properly despite the compressible behavior of the paste, which causes a slower transient response when using a plunger velocity controller. The extrusion force controller utilized for extrusion-on-demand operates in a closed-loop feedback control scheme; therefore, by selecting a "desired" closed-loop time constant, the delay time for trajectory start and stop is fixed and independent of paste properties. An added benefit of the hybrid controller is that the gap defects caused by the release of entrapped air bubbles are mitigated. The release of entrapped air bubbles within a part can be catastrophic for deposition-based additive manufacturing if the gap defect is large enough to cause structural failure. Minimizing these defects is essential since there is the potential for air bubble entrapment with any paste-deposition based process. Air bubble release compensation reduced the severity of defects caused by the release of an air bubble during part fabrication by utilizing the

hybrid force-velocity controller. The hybrid extrusion force-velocity control scheme has been implemented in a triple-extruder FEF machine and successfully demonstrated to fabricate monolithic and FGM parts.

Extrusion-on-demand requires the use of a trajectory-based method for "stop" commands to ensure extrusion will stop at the desired location by accounting for the settling time associated with paste decompression within the syringe as the plunger retracts. Extrusion "start" commands can be successfully implemented with either the dwell-based method or the trajectory-based method, by setting the closed-loop time constant of the extrusion force controller; however, the dwell-based method is preferred because it is relatively easy to implement.

8. ACKNOWLEDGEMENTS

9. REFERENCES

[1] Hilmas, G., Lombardi, J., and Hoffman, R., 1996, "Advances in the Fabrication of Functional Graded Materials using Extrusion Freeform Fabrication," Proceedings of Solid Freeform Fabrication Symposium, Austin, TX, pp. 319-324.

[2] Griffith, M.L. and Halloran, J.W., 1996, "Freeform Fabrication of Ceramics via Stereolithography," Journal of the American Ceramic Society, 79(10), pp. 2601–2608.

[3] Bandyopadhyay, A., Panda, P., Agarwala, M., Danforth, S., and Safari, A., 2000, "Processing of Piezocomposites by Fused Deposition Technique," Journal of the American Ceramic Society, 80(6), pp. 1366-1372.

[4] Cima, M., Oliveira, M., Wang, H., Sachs, E., and Holman, R., 2001, "Slurry-Based 3DP and Fine Ceramic Components," Proceedings of Solid Freeform Fabrication Symposium, Austin, TX, pp. 216-223.

[5] Kruth, J., Mercelis, P., Froyen, L., and Rombouts, M., 2004, "Binding Mechanisms in Selective Laser Sintering and Selective Laser Melting," Proceedings of Solid Freeform Fabrication Symposium, Austin, TX, pp. 44-59.

[6] Leu, M.C., Pattnaik, S., and Hilmas, G.E., 2012, "Investigation of Laser Sintering for Freeform Fabrication of Zirconium Diboride Parts," Journal of Virtual and Physical Prototyping, 7(1), pp. 25-36.

[7] Cesarano III, J., Segalmen, R., and Calvert, P., 1998, "Robocasting Provides Moldless Fabrication from Slurry Deposition," Ceramics Industry, 148(4), pp. 94-102.

[8] Crump, S., 1992, Apparatus and Method for Ceramic Three-Dimensional Objects, U.S. Patent No. 5121329.

[9] Stampfl, J., Cooper, A., Leitgeb, R., Cheng, Y., and Prinz, F., 2001, "Shape Deposition Manufacturing of Microscopic Ceramic and Metallic Parts Using Silicon Molds, U.S. Patent, No. 6242163.

[10] Tang, L., Ruan, J., Landers., R.G., and Liou, F., 2008, "Variable Powder Flow Rate Control in Laser Metal Deposition Processes," ASME Journal Manufacturing Science and Engineering, 130(4), pp. 041016.

[11] Huang, T., Mason, M.S., Hilmas, G.E., and Leu, M.C., 2006, "Freeze-form Extrusion Fabrication of Ceramic Parts," International Journal of Virtual and Physical Prototyping, 1(2), pp. 93-100.

[12] Mason, M.S., Huang, T., Landers, R.G., Leu, M.C., and Hilmas, G.E., 2009, "Aqueous-Based Extrusion of High Solids Loading Ceramic Pastes: Process Modeling and Control," Journal of Materials Processing Technology, 209(6), pp. 2946-2957.

[13] Huang, T., Mason, M.S., Hilmas, G.E., and Leu, M.C., 2009, "Aqueous Based Freeze-form Extrusion Fabrication of Alumina Components," Rapid Prototyping Journal, 15(2), pp. 88-95.

[14] Zhao, X., Landers, R.G., and Leu, M.C., 2010, "Adaptive Extrusion Force Control of Freeze-Form Extrusion Fabrication Processes," ASME Journal of Manufacturing Science and Engineering, 132(6), pp. 064504.

[15] Doiphode, N.D., Huang, T., Leu, M.C., Rahaman, M.N., and Day, D.E., 2011, "Freeze Extrusion Fabrication of 13-93 Bioactive Glass Scaffolds for Bone Repair," Journal of Material Science: Materials in Medicine, 22(3), pp. 515-523.

[16] Li, M., Tang, L., Xue, F., and Landers, R.G., 2011, "Numerical Simulation of Ram Extrusion Process for Ceramic Materials," Proceedings of Solid Freeform Symposium, Austin, TX, pp. 290-308.

[17] Oakes, T., Kulkarni, P., Landers, R.G., and Leu, M.C., 2009, "Development of Extrusion-on-Demand for Freeze-form Extrusion Fabrication Processes," Proceedings of Solid Freeform Symposium, Austin, TX, pp. 206-218.

[18] Kennedy, J. and Eberhart, R.C., 1995, "Particle Swarm Optimization," IEEE International Conference on Neural Networks, Perth, Australia, pp. 1942–1948.

[19] Alleyne, A. and Liu, R., 2000, "A Simplified Approach to Force Control for Electro-Hydraulic Systems," Control Engineering Practice, 8(12), pp. 1347-1356.

SUMMARY

The general tracking control methodology was implemented for a plunger velocity controller and an extrusion force controller on the triple-extruder Freeze-form Extrusion Fabrication machine. A hybrid controller was designed and to regulate extrusion on demand and to compensate for air bubble release. This controller was used in conjunction with a tool path planning program in order to fabricate complex geometry parts. Green ceramic parts were fabricated in a temperature of -10°C using aluminum oxide paste and a functionally graded part was fabricated using colored calcium carbonate paste to illustrate the capability of the hybrid controller.

The effect of extrusion velocity on material transport delay due to static mixing was investigated and it was found to be repeatable; however, the additional transition delay between composition changes resulted in uncertainty in the theoretical time delay. A one-dimensional gradient control algorithm was developed and implemented to apply horizontal and vertical gradients to a monolithic part and its capability was demonstrated on simple geometry parts. This algorithm was developed further to fabricate more complex three-dimensional gradients by splicing together multiple parts of individual (discrete) compositions, as demonstrated with the hybrid extrusion force-velocity controller by fabricating a radially-graded FGM part.

CONCLUSIONS

General tracking control of the plunger velocity and extrusion force rejected disturbances such as Coulomb friction and inconsistencies in the paste. The plunger velocity controller could achieve minimum velocities near the resolution of the linear servo motors, which allowed for composition ratios of approximately 1:9 with a two-paste system. The extrusion force controller was stable from 20 N to the operational limit of the servo motors (1000 N); therefore, it was adequate for extrusion force control in the FEF process since the typical extrusion force does not exceed 800 N for the process parameters, such as table speed and standoff distance, used in this study. Air bubble release compensation allowed the hybrid controller to reduce the severity of defects caused by the release of air bubbles by switching from plunger velocity control to extrusion force after detecting a drop in measured extrusion force. Without the hybrid controller, this compensation would not be possible with a plunger velocity controller alone.

The hybrid control scheme was successfully implemented and used with an open source tool path planning software to fabricate single and multiple material parts on the FEF machine. Reasonably complex geometry parts were fabricated with unsupported overhangs of up to 45° without structurally significant defects. Minor process parameter tuning was necessary when using the tool path planning software, but results were consistent for separate batches of paste once these parameters were tuned properly for a set standoff distance (400 μm in this study).

The use of an inline static mixing unit was determined to be feasible for grading between two pastes; however, the transport delay associated with changing compositions will require purging excess material if the time required for deposition of a given composition is less than the time delay. This is to ensure that the output composition contains no transitional material from mixing with the previous composition.

BIBLIOGRAPHY

[1] Griffith, M. L. and Halloran, J. W., 1996, "Freeform Fabrication of Ceramics via Stereolithography," Journal of the American Ceramic Society, 79, pp. 2601–2608.

[2] Bandyopadhyay, A., Panda, P., Agarwala, M., Danforth, S., and Safari, A., 2000, "Processing of Piezocomposites by Fused Deposition Technique," Journal of the American Ceramic Society, 80(6), pp. 1366-1372.

[3] Cima, M., Oliveira, M., Wang, H., Sachs, E., and Holman, R., 2001, "Slurry-Based 3DP and Fine Ceramic Components," Proceedings of Solid Freeform Fabrication Symposium, Austin, TX, pp. 216-223.

[4] Kruth, J., Mercelis, P., Froyen, L., and Rombouts, M., 2004, "Binding Mechanisms in Selective Laser Sintering and Selective Laser Melting," Proceedings of Solid Freeform Fabrication Symposium, Austin, TX, pp. 44-59.

[5] Leu, M.C., Adamek, E., Huang, T., Hilmas, G. E., and Dogan, F., 2008, "Freeform Fabrication of Zirconium Diboride Parts Using Selective Laser Sintering," Proceedings of Solid Freeform Fabrication Symposium, Austin, TX, pp. 194-205.

[6] Hilmas, G., Lombardi, J., and Hoffman, R., 1996, "Advances in the Fabrication of Functional Graded Materials Using Extrusion Freeform Fabrication," Proceedings of Solid Freeform Fabrication Symposium, Austin, TX, pp. 319-324.

[7] Cesarano III, J., Segalmen, R., and Calvert, P., 1998, "Robocasting Provides Moldless Fabrication from Slurry Deposition," Ceramics Industry, 148, pp. 94-102.

[8] Crump, S., 1992, Apparatus and Method for Ceramic Three-Dimensional Objects, U.S. Patent No. 5121329.

[9] Stampfl, J., Cooper, A., Leitgeb, R., Cheng, and Y., Prinz, F., 2001, "Shape Deposition Manufacturing of Microscopic Ceramic and Metallic Parts Using Silicon Molds, U.S. Patent, No. 6242163.

[10] Tang, L., Ruan, J., Landers., R.G., and Liou, F., 2008, "Variable Powder Flow Rate Control in Laser Metal Deposition Processes," ASME Journal Manufacturing Science and Engineering, 130(4), pp. 041016.

[11] Huang, T., Mason, M. S., Hilmas, G. E., and Leu, M.C., 2006, "Freeze-form Extrusion Fabrication of Ceramic Parts," International Journal of Virtual and Physical Prototyping, 1(2), pp. 93-100.

[12] Mason, M. S., Huang, T., Landers, R. G. , Leu, M. C., and Hilmas, G. E. , 2009, "Aqueous-Based Extrusion of High Solids Loading Ceramic Pastes: Process

Modeling and Control," Journal of Materials Processing Technology, 209(6), pp. 2946-2957.

[13] Huang, T., Mason, M. S., Hilmas, G. E., and Leu, M. C., 2009, "Aqueous Based Freeze-form Extrusion Fabrication of Alumina Components," Rapid Prototyping Journal, 15(2), pp. 88-95.

[14] Zhao, X., Landers, R. G., and Leu, M. C., 2010, "Adaptive Extrusion Force Control of Freeze-Form Extrusion Fabrication Processes," ASME Journal of Manufacturing Science and Engineering, 132(6), pp. 064504.

[15] Doiphode, N. D., Huang, T., Leu, M.C., Rahaman, M.N., and Day, D.E., 2011, "Freeze Extrusion Fabrication of 13-93 Bioactive Glass Scaffolds for Bone Repair," Journal of Material Science: Materials in Medicine, 22(3), pp. 515-523.

[16] Oakes, T., Kulkarni, P., Landers, R.G., and Leu, M.C., 2009, "Development of Extrusion-on-Demand for Freeze-form Extrusion Fabrication Processes," Proceedings of Solid Freeform Symposium, Austin, TX, pp. 206-218.

[18] Jackson, T., Patrikalakis, N., Sachs, E., and Cima, M., 1998, "Modeling and Designing Components with Locally Controlled Composition," Proceedings of Solid Freeform Symposium, Austin, TX, pp. 259-266.

[19] Kou, X., and Tan, S., 2005, "A Hierarchical Representation for Heterogeneous Object Modeling," Computer-Aided Design, 37, pp. 307-319.

[20] Siu, Y.K. and Tan, S.T., 2002, "'Source-based' heterogeneous solid modeling," Computer-Aided Design, 34, pp. 41-45.

[21] Xu, A. and Shaw, L., 2004, "SFF-Oriented Modeling and Process Planning of Functionally Graded Materials using a Novel Equal Distance Offset Approach," Proceedings of Solid Freeform Symposium , Austin, TX, pp. 544-552.

VITA

Bradley Kenneth Deuser was born in St. Louis, Missouri. He attended East Central College for two years before transferring to the Missouri University of Science and Technology (formerly the University of Missouri – Rolla). During his undergraduate studies he completed a six-month co-op with Metal Container Corporation as a Technical Development intern, and was an active member and officer in Pi Tau Sigma – the International Mechanical Engineering Honor Soceity. He received his Bachelor of Science degree in Mechanical Engineering and a minor in Material Science in May of 2010. He worked as a Design Engineer with Grain Systems Incorporated for a three-month internship before continuing his education with Missouri S&T and receiving his Masters of Science degree in Mechanical Engineering in August of 2012.

Permanent Address:

433 Sue Lane

Saint Clair, Missouri, 63077

Email:

bkdeuser@gmail.com